EFFECT OF ANNEALING ON THE MORPHOLOGICAL AND OPTOELECTRONIC PROPERTIES OF $CH_3NH_3PbI_3$ THIN FILMS FOR PEROVSKITE SOLAR CELL APPLICATIONS.

A Thesis Submitted to the Department of Materials Science and Engineering

African University of Science and Technology

In Partial Fulfilment of the Requirements for the Degree of

MASTER OF SCIENCE in Materials Science and Engineering

BY

FRANCIS AKUDAGO APAM (40724)

Abuja-Nigeria

SUPERVISOR**: Dr VITALIS CHIOH ANYE**

March, 2021

CERTIFICATION

This is to certify that the thesis titled "Effect of Annealing on the Morphological and Optoelectronic Properties of $CH_3NH_3PbI_3$ Thin Films for Perovskite Solar Cell Applications**"** Submitted to the Department of Materials Science and Engineering, African University of Science and Technology (AUST), Abuja, Nigeria for the award of the Master Degree is an original research carried out by **Francis Akudago Apam** in the Department of Materials Science and Engineering.

© 2021

Francis Akudago Apam

ALL RIGHTS RESERVED

EFFECT OF ANNEALING ON THE MORPHOLOGICAL AND OPTOELECTRONIC PROPERTIES OF $CH_3NH_3PbI_3$ THIN FILMS FOR PEROVSKITE SOLAR CELL APPLICATIONS

BY

Francis Akudago Apam

A THESIS SUBMITTED TO THE DEPARTMENT OF MATERIALS SCIENCE AND ENGINEERING

RECOMMENDED: _____

Supervisor: Dr Vitalis Chioh Anye

_____

Member: Mr. Yusuf Olanrewaju

_____

Prof. Peter Azikiwe Onwualu

Head, Department of Materials Science and Engineering

APPROVED: _____

Chief Academic Officer

31st March, 2021

_____

Date

ABSTRACT

Organolead Trihalide Perovskites (OTPs) is one of the third generations' photovoltaic technologies which have achieved excellent power conversion efficiency (PCE) of 3.8% in 2009 to 23.7% in 2018, just within nine years of its advent. High extinction coefficient, high charge mobility, long carrier diffusion distance and long carrier lifetime are some essential factors that enable perovskite materials to be used as electron/hole transport layer aside from acting as a light-absorbing layer. However, numerous factors such as annealing temperature, solution concentration, precursor composition, and the choice of solvent affect the film morphology. In this work, methylammonium lead iodide thin films were prepared using two different deposition techniques, one-step spin-coating technique (OSSC) and two-step spin coating technique (TSSC). The variation of the temperature and the type of fabrication approach affects the surface morphology of the films. The surface morphology obtained from SEM revealed that perovskite films produced by OSSC had large pinholes and non-uniform coverage, while thin films obtained by the TSSC method exhibited full-coverage with little or no pinholes implying enhanced film performance which is consistent with that which is reported by Swati (Chaudhary et al., 2020). As the temperature changes, the morphology was observed to yield full coverage at 100 ^{0}C than at lower (80 ^{0}C) or higher (120 ^{0}C) temperatures. By comparing device performance for OSSC and TSSC methods, it was found that TSSC deposited-based perovskite thin films demonstrated a significant enhancement in performance. This could be as a result of high absorbance, lesser trap density, low current leakage, larger carrier mobility arising from moderate temperature and better surface morphology. Characterization obtained from the UV/VIS Spectrometry of the perovskite thin films showed high absorbance for TSSC than for OSSC at all temperatures. It also indicated that for both TSSC and OSSC higher absorbance was observed at 100 ^{0}C. This could be attributed to the fairly moderate temperature that does not cause film degradation leading to strong and broad spectra. Sheet Resistance measurements using the Four-Point Probe indicated lower resistivity at 100 ^{0}C (7.0556Ω/sq and 7.9816Ω/sq) for both TSSC and TSSC techniques respectively which resulted in the high current generation. However, the sheet resistance for TSSC was fairly lower than that of the OSSC at the same temperature yielding high device (thin films) performance which is consistent to what was observed by Mwende Mbilol et al., Barnett et al., 2016 (11.66% PCE).

Keywords: Photovoltaics, Solar cell, Perovskite, Methylammonium Iodide, Lead Iodide, Sheet Resistivity, Morphology, Pinholes

ACKNOWLEDGEMENT

I give thanks to the Almighty God for all that He has done for me**.** Your power, strength, wisdom, provision, and divine protection are the reasons why I sailed through this research work successfully. I am who I am because of Your Love, Compassion and Mercies.

My heartfelt gratitude goes to Dr. Vitalis Chioh Anye, my supervisor for his devoted time, guidance, patience, encouragement, and support which led to the success of this research. His interest and enthusiasm for science and renewable energy was a source of inspiration as he believed in my ability and commitments in carrying out any responsibility assigned to me.

I wish to express my appreciation to Mr. Yusuf Olanrewaju and Mr. Daniel Amune for their time and valuable contributions which steered me in the right part. I cannot remain adamant to thank my mentor, Professor Winston Oluwole Soboyejo for his insightful encouragement and guidance offered before the start, during and at the end of my research work.

I remain indebted to all my friends, well-wishers, classmates and my co-project students; Nalyanya Fred and Ajah Chimah Jamael for their support. I also wish to thank the entire laboratory technologists at the African University of Science and Technology (AUST) for their technical support. I also thank my sponsors AUST and the Nelson Mandela Institution (NMI) for their support.

Finally, my profound gratitude goes to my family (the Alazuga family, my lovely parents and siblings) for their love, financial support, encouragement, and prayers which propelled me through school. To Rev. Akpaliok Lincoln and his wife, I say thank you for the spiritual support. I say thank you to my sweetheart; Arongo Rosina for your love, time, and patience exercised throughout my study. God bless you all!

Table of Contents

List of Tables

List of Figures

CHAPTER ONE (1)

1.0 INTRODUCTION

1.1. BACKGROUND OF THE STUDY

The demand for energy for the sustainable development of our society today is largely dependent on the rampant increase in our population. The total number of people living in the world is about 7.8 billion as of March 2020. It took over 2 million years of human history for the world's population to reach 1 billion, and only 200 more years to reach 7 billion. It took over 2 million years of human history for the world's population to reach 1 billion, and only 200 more years to reach 7 billion. With the increasing global energy consumption coupled with climatic changes and environmental pollution, traditional fossil energy sources are limited to sustainably meet our demand (T.-B. Song et al., 2015; D. Zhou et al., 2018). The utilization of clean, renewable energy resources has become imperative for this development. Among the numerous types of new energy technologies, photovoltaic is one of the most promising renewable sources of power to meet the future challenges of energy needs(D. Zhou et al., 2018). This has attracted a lot of attention of researchers to provide clean and affordable energy which is considered one of the Sustainable Development Goals (SDGs). A solar cell is a device that converts light energy directly into electrical energy through photovoltaic or photochemical reactions. Fortunately, solar power is the most abundant energy source in the world in which Africa has a greater advantage. The total estimated energy from the sun for a year is about $1.5 \times 10^{18} kWh$ which is greater than that of the known reserves of oil $(1.4 \times 10^{15} kWh)$, gas $(1.75 \times 10^{15} kWh)$ and coal which is approximately $5.5 \times 10^{15} kWh$. The most dominant photovoltaic solar devices for efficient power conversion for commercial purposes are crystalline silicon solar cells. However, the cost of fabrication involves pure and expensive materials, high-technology processing techniques, and high-temperature processing which renders crystalline silicon solar cells not economically viable for many applications. The solution processing technique of solar modules is an alternative approach that offers the opportunity to reduce costs and provide better power conversion efficiency. The third generation energy technologies involved in the fabrication process of solar cells through solution processing, low-temperature processes which reduces the production cost include; organic solar cells, quantum dot solar cells, dye-sensitized solar cells

and polymer solar cells (Liyan Yang et al., 2016). However, their limited absorption and low carrier mobility limit their achieving commercially viable device efficiencies.

1.2. JUSTIFICATION OF WORK

Long-term stability, hysteresis, environmental factors due to the presence of toxic metals (lead), high cost and difficulties in fabrication of large area and/or flexible devices are the major challenges that hinder the photovoltaic solar cell performance (Djurišić et al., 2017b). Perovskites are a third-generation organic-inorganic solar cell that accounts for a broad spectrum of concepts, ranging from low-cost low-efficiency systems to high-cost high-efficiency systems (Ibn-Mohammed et al., 2017). High extinction coefficient, high charge mobility, long carrier diffusion distance and long carrier lifetime are some essential factors that enable perovskite materials to be used as electron/hole transport layer aside from acting as a light-absorbing layer (D. Zhou et al., 2018). However, external conditions like temperature and light affect the perovskite solar cell performance layers such as $CH_3NH_3PbI_3$, spiro-OMeTAD etc. It has been reported that at high temperature say; 85 ° C, I− and $CH_3NH_3^{+¿¿}$ (MA+) diffused into the spiro-OMeTAD layer in the form of $CH_3NH_3I_3$ (MAI). The diffused I− ions prevented oxidation of spiro-OMeTAD, thereby degrading the electrical properties of spiro-OMeTAD. Since ion diffusion can occur during outdoor operation, the structural design of PSCs must be considered to achieve long-term stability. To protect the perovskite from moisture, various hole-transporting materials (HTMs), such as hydrophobic and inorganic materials, have been developed resulting in increased long-term stability (Li, M.H, 2015; Bai, 2016).

Extensive research has been carried on hybrid organic-inorganic perovskite solar cells (HOIPSCs) since its advent in 2009. PSC offers the advantages of a simple and economical manufacturing process and outstanding energy conversion efficiency (F. Chen, 2015; Conings, 2015; D.M. Chapin, C. S. Fuller, 1954; Hwang, I., Jeong, I., Lee, J., K, M. J. & Yong, 2015; M. A. Green, K. Emery, Y. Hishikawa, W. Warta, 2016). Recently, there have been reports of PSCs with efficiencies exceeding 22%. However, the long-term stability of these types of solar cells prevents their commercialization (Habisreutinger, 2014). A high-efficiency PSCs is $MAPbI_3$, $Cs_x(MA_yFA_{1-y})(1-x)Pb¿$, with respective electron- and hole-selective contacts such as mesoporous TiO2 (m-TiO_2) and 2, 2′, 7,7′-tetrakis *N*,*N*-di-*p*-methoxyphenylamine)-9,9-spiro-bi-fluorene (spiro-OMeTAD) (Conings, 2015, Niu, 2014).

These PSCs are often considered ineffective. It is widely known that the main reasons for the deterioration of solar cell performance are associated with the following external conditions such as moisture (Leijtens, 2013, Bae, 2016), temperature (Azpiroz, J. M., et al 2015, Yang, J., et al, 2015), UV light(Li, M.H, 2015, Bai, 2016), etc. Besides, problems associated with intrinsic factors such as ion migration (Etgar, 2012, Azpiroz, J. M., 2015), interfacial reactions (Yang, J., 2015), etc., have been pointed out as a cause of insufficient long-term stability of PSC. Solar cells must be stable against the above external conditions to function efficiently for decades. Thermal stability is essential under normal operating conditions, especially during long-term operation, since solar cell temperatures can reach 85 ° C or more.

1.3. PROBLEM STATEMENT

Among the various solution processing techniques, the one-step technique is the simplest for the growth of perovskites. However, numerous factors such as; annealing temperature, solution concentration, precursor composition, and the choice of solvent affect the film morphology, mechanical and optoelectronic properties. Low or high temperature caused adverse effects leading to degradation of the perovskite layer and hence reduces its stability and efficiency. This thesis work is therefore focused on studying the effect of annealing on the morphological and optoelectronics properties of the thin films for optimum performance for perovskite solar cell applications. Both one-step and two-step spin coating techniques would be adapted for the deposition under varied temperatures of annealing to obtain the optimum temperature for enhanced device performance.

1.4.0 OBJECTIVES

1.4.1 General Objective

This research work is focused on optimizing stability by studying the effect of annealing on the morphological and optoelectronic properties of $CH_3NH_3PbI_3$ thin films for perovskite solar cell applications.

1.4.2 Specific Objectives

The specific targets of the thesis are as follows;

- To obtain $CH_3NH_3PbI_3$ from CH_3NH_3I and PbI_2 powders by one-step and two-step solution spin coating methods.
- To study the thermal annealing effect on the perovskite ($CH_3NH_3PbI_3$) active layer for a temperature range of 80 ^{0}C to 120 ^{0}C in steps of 20 ^{0}C.
- To study the changes in surface morphology and optoelectronic properties by the use of Scanning Electron Microscopy and UV/Vis Spectroscopy.
- To measure the sheet resistance of perovskite thin films formed using a four-point probe.

1.5. OUTLINE OF THESIS

This research is structured into the following chapters;

Chapter One gives a general introduction to the current needs of energy, solar power and the technologies involved and perovskite solar cells. The aim and objectives of this research work are also specified in this chapter.

Chapter Two is a literature review on the world's energy needs, the energy challenges facing Africa and how the economy is being affected. It also provides a review of the fundamentals and evolution of photovoltaic and solar cells.

Chapter Three offers a detailed review of perovskite solar cells (PSCs) and works by researchers in the field.

Description of detail experimental procedure carried out is contained in Chapter Four (4).

The results obtained after the characterization and plotting of essential graphs are presented in Chapter Five (5). Interpretation and discussion of the results are also included here. The conclusion and recommendations for future work are offered in Chapter Six.

CHAPTER TWO (2)

2.0 LITERATURE REVIEW

2.1 ENERGY NEEDS OF THE WORLD AND AFRICA

Energy remains a major area of concern because it is needed in almost all sectors of life. The driving force for the economic development, medical advancements, improved nutrition, security services, and social development of any nation depends on energy. According to the United Nations Population Division, the total number of people living today is about 7.8 billion as of November 2020 (estimates elaborated by world meter). It took over 2 million years of human history to reach 1 billion people in the world, but it took only 200 years to reach 7 billion people. The UN Population Department estimates there will be about 9.7 billion people on the planet by 2050(Keilman, 1998; Graham Zabel, 2009). The increase in population places a high demand on energy to meet the advances in the various services mentioned above.

A major challenge has been the high cost of production, conversion efficiency, storage materials and better media for its transport. A lot of researchers reported the improvement in all these challenges but none has seen full commercialization. Solar cells have emerged to provide a reliable alternative to fossil fuels, providing large amounts of renewable energy at affordable prices.

The International Energy Agency (IEA) and the Energy Information Agency (EIA) have announced that global total energy consumption will start at 549 trillion BTU in 2012, based on past and current energy consumption trends to about 815 quadrillions BTUs in 2040, an increase of 48% (International Energy Agency, 2016). Much of this global energy demand is produced in developing countries other than the OECD (Organisation for Economic Cooperation and Development) nations, which include Africa. The main factor that determines our energy consumption forecasts is population growth. It is predicted that non-OECD demand for energy will rise by 71% from 2012 to 2040, compared to an increase of 18% in OECD nations, refer to Figure 1.

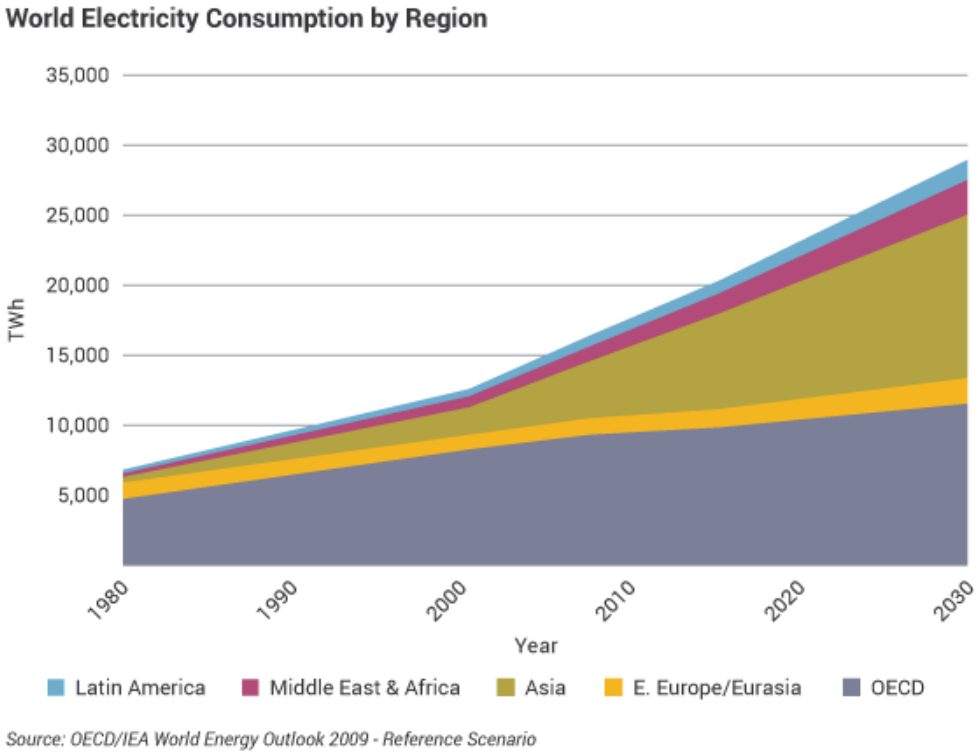

Figure 1: *World Electricity Consumption by region (World-nuclear association, 2017).*

In sub-Saharan Africa, two-thirds of the population thus; more than 620 million people live without electricity. The economy of Africa is not fully developed since Africa has not been able to meet its present energy need. Approximately 40% of Africa's surface receives over 2000 kilowatts per hour of solar energy annually (Z. Liu, 2015) making Africa the world's best potential for solar power. It is therefore imperative for Africa to take advantage of her rich solar energy supply to meet her growing population and energy demand for improved economic development (Jimoh, 2014). Globally, the sun's energy supply needs to be harnessed efficiently and cost-effectively to meet the projected increase in global energy demand.

2.1 Solar Energy

Solar energy is a renewable energy source emitted from the sun in the form of electromagnetic radiation such as light and heat onto the earth or space. Solar power is the cleanest and most abundant renewable energy source, and the United States has one of the substantial solar energy resources in the world. Different types of solar energy technologies can be used to convert/trap this energy for different applications including; generation of electricity, providing light or comfortable conditions, as well as heating water for domestic,

commercial or industrial uses. The Sun emits 3.8 x 10^{26} watts of electromagnetic power from gamma-ray to radio wavelengths, with most of the energy emitted in the visible light spectrum between 400nm and 700nm (Sten Odenwald's, 2017). Exactly 3.8 x 10^{26} joules of solar energy are emitted at each second with about 6.33 x 10^{7} W/m^{2} intensity of solar radiation. Averagely, one square meter of land is exposed to enough sunlight to generate 1,700 kWh of electricity per year (ITACA, 2017). The more the Sun's rays spread out into space, the less intense the radiation becomes, with only a fraction of the emitted energy reaching the earth's surface. These reductions are due to absorption and scattering by the earth's surface-atmosphere caused by, the ozone, water vapor, nitrogen, oxygen, and carbon dioxide that prevents some of the ultraviolet (UV) and infrared (IR) parts of the sun's spectrum from reaching the earth's surface.

Air mass is a large mass of air, the temperature and humidity of which are practically the same in the horizontal direction at all altitudes.

Air Mass is a large body of air whose properties of temperature and moisture content (humidity), at any given altitude, are mostly uniform in any horizontal direction (National Geographic Society, 2017). The air mass coefficient (AM1.5) is an index used to determine the effective electromagnetic radiation emitted by the sun at sea level. It denotes the maximum amount of energy that is available to be converted into an electrical current by a solar cell. The maximum irradiance peak in the AM1.5 spectrum is in the visible light region, nonetheless, an ideal solar cell should be able to convert the whole part of the spectrum to maximize the yield of the current generated (Bastiani, 2016).

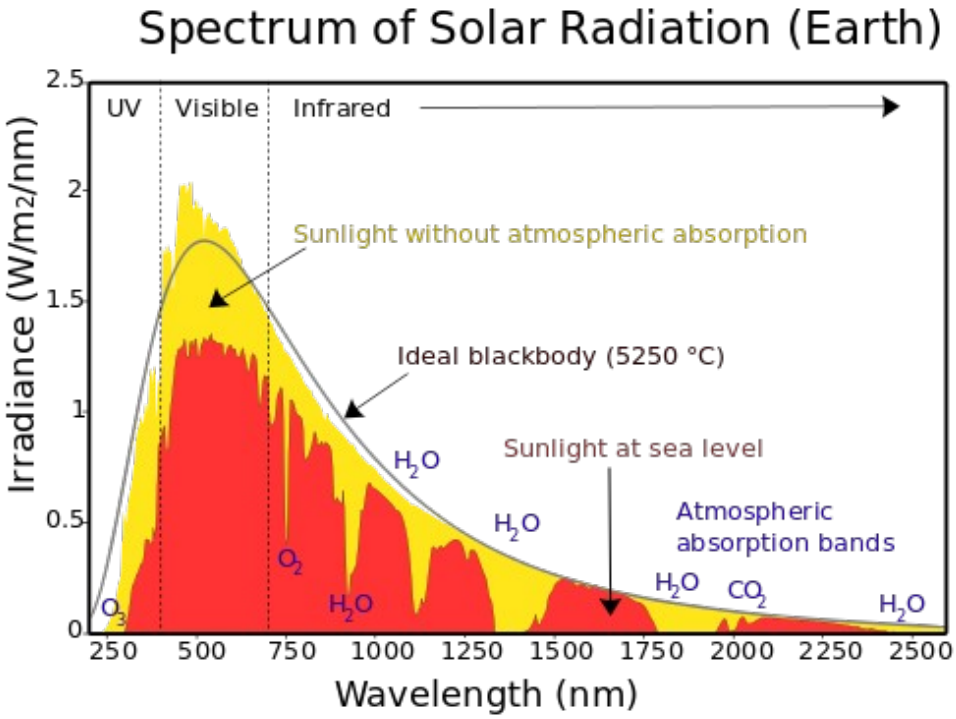

Figure 2: *Solar irradiance spectrum and atmospheric absorbing gases from 240 nm to 2.5 nm,(Marcin Majka & Tomasz M. Majka, 2013)*

2.2 Photovoltaic

Photovoltaics (PVs) also called solar cells convert sunlight directly into electricity at an atomic level. Photovoltaics are clean and renewable energy source that uses sunlight to generate electricity. It works on the principle of the photoelectric effect, where certain materials can absorb photons. It glows with light and emits electrons. When these free electrons are captured, the result is an electric current that can be used as electricity(Green Energy, 2015). When light rays of suitable frequencies fall on semiconductor materials, some of the photons in the beam are absorbed by the semiconductor crystal, causing a significant amount of free electrons and holes in the crystal. Recombination of the free electrons and holes can occur if there is no driving force; hence the solar cell must provide an internal electric field to transport the electrons and holes in opposite directions. Light absorption and charge separation are the two fundamental processes of the PV effect forming the basis of all inorganic PV cells. This is the basic principle of obtaining energy through the photoelectric effect (Vatansever et al., 2012). The current is generated in the depletion zone or PN junction. A PN junction is where electrons from N-type silicon occupy holes in P-type electrons. An electron is displaced producing a free electron and a hole when the photons of the beam are

absorbed by one of the N-type silicon atoms. When the metal wire is connected to the cathode (N-type silicon), anode (P-type silicon), free electrons are attracted to the free holes causing electrons after passing through the depletion layer to flow from the N-type layer to the P-type layer and back through the wires outside the N-type layer, creating a flow of electricity (American Chemical Society, 2014).

Solar cells have evolved over the years due to different technologies, in a bid to convert the sun's energy to power efficiently with the least cost. The history of solar cells can be divided into three generations namely; first generation, second generation and third generation.

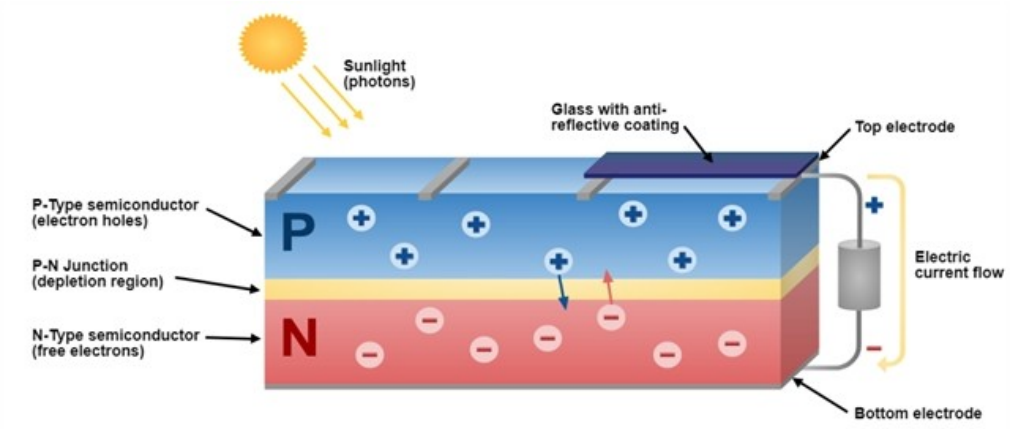

Figure 3*: Layers and working principle of a silicon solar cell (Vatansever et al., 2012)*

2.3 Electrical Characteristics of Photovoltaic

Three important parameters characterize the performance of a photovoltaic cell. These are the short circuit current (I_{SC}), the open-circuit voltage (V_{SC}), and the fill factor (FF) (Jasim, 2015)

2.3.1 Short Circuit Current

This is the current through the solar cell when the voltage across the solar cell is zero (that is, when the solar cell is short-circuited). Short circuit current (Isc) occurs due to the generation and collection of light-generated carriers (Baghzouz, 2017). The optical properties of the solar cell, the power of the incident light, the spectrum of the incident light, the area of the solar cell and the collection probability of the solar cell are all factors that determine Isc. Short-circuit current density (Jsc) is used instead of short-circuit current to remove the dependency of the solar cell area on Isc. The maximum current that a solar cell can provide is highly dependent on the optical properties of the solar cell, such as absorption in the absorber

layer and reflection (Chritiana Honsberg & Stuart Bowden, 2017). The collection probability depends mainly on surface passivation of the solar cell to prevent surface recombination of photo-excited electron-hole pairs (Ruy et al, 2012). The maximum current that can be drawn from a solar cell is the short circuit current (Alternative Energy, 2017).

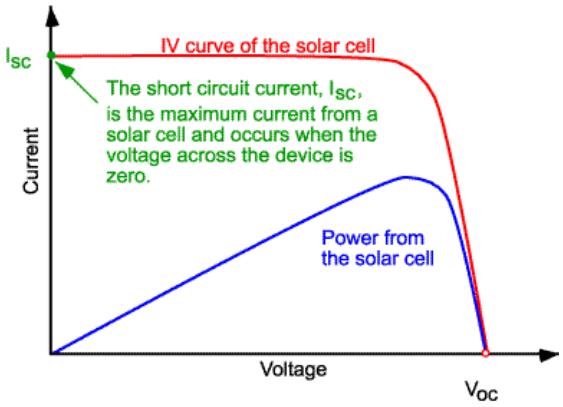

Figure 4: *Short-circuit current diagram*

The short circuit current density (J_{SC}) depends on generation rate and the diffusion length of electrons and holes which is shown in the equation below;

$$J_{SC} = qG(\ln + Lp) \quad \text{.....Equation 1}$$

Where G is the generation rate, q represents the absolute value of the electron charge, and Ln and Lp are the electron and hole diffusion lengths respectively (Chritiana Honsberg & Stuart Bowden, 2017).

2.3.2 Open-circuit voltage

The maximum available voltage of solar cells when not connected to any load (zero current) is termed open-circuit voltage (V_{OC}) (Alternative Energy, 2017). The total rate of photo generation in the solar cell is equal to the rate of recombination so that no current circulates through the circuit. The open circuit voltage corresponds to the forward bias value in the solar cell due to the bias in the connection of the solar cell to the current generated by the light. Equating the net current to zero in the solar cell equation yields the equation for Voc as;

$$V_{OC} = \frac{nkT}{q} In(\frac{I_L}{I_O} + 1)$$ ……*Equation 1*

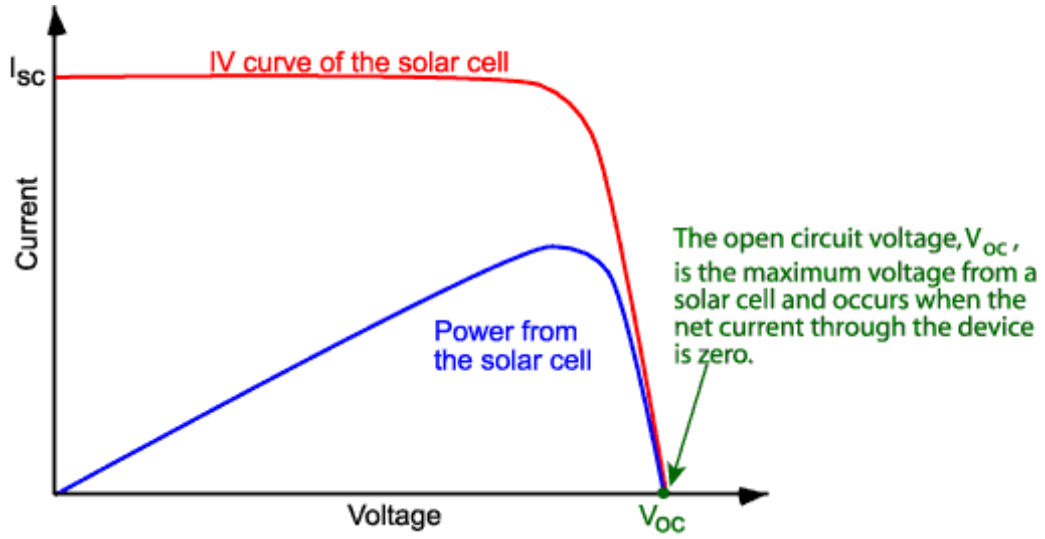

Figure 5: *Short Circuit Current diagram*

Where K is the Boltzmann's constant, T is the absolute temperature, n is the ideality factor, q is the absolute value of the electron charge, I_L is the photo-generated current and Io is the reverse saturation current or "dark saturation current". Therefore open-circuit voltage is the measure of the recombination of a device.

2.3.3 Fill factor

The "fill factor" (FF) is a measure of the quality of a solar cell, it determines the maximum power from a solar cell when combined with Voc and Isc (Christiana Honsber & Stuart Bowden, 2017). The FF is defined as the ratio of the maximum power (Imp x Vmp) from the solar cell to the product of Voc and Isc (the theoretical power) (Alternative Energy, 2017). When analyzed graphically, the FF is the area of the largest rectangle which can fit in the I-V curve. It can be computed from the equation below;

$$FF = \frac{V_m I_m}{I_{sc} V_{oc}} \quad \text{.....Equation 2}$$

Where V_m and I_m are the maximum output voltage and current respectively

A solar cell with a higher voltage has a larger possible fill factor, the closer the fill factor is to unity, the more power the PV can provide. Fill factors range from 0.5 to 0.82 (National Instruments, 2017).

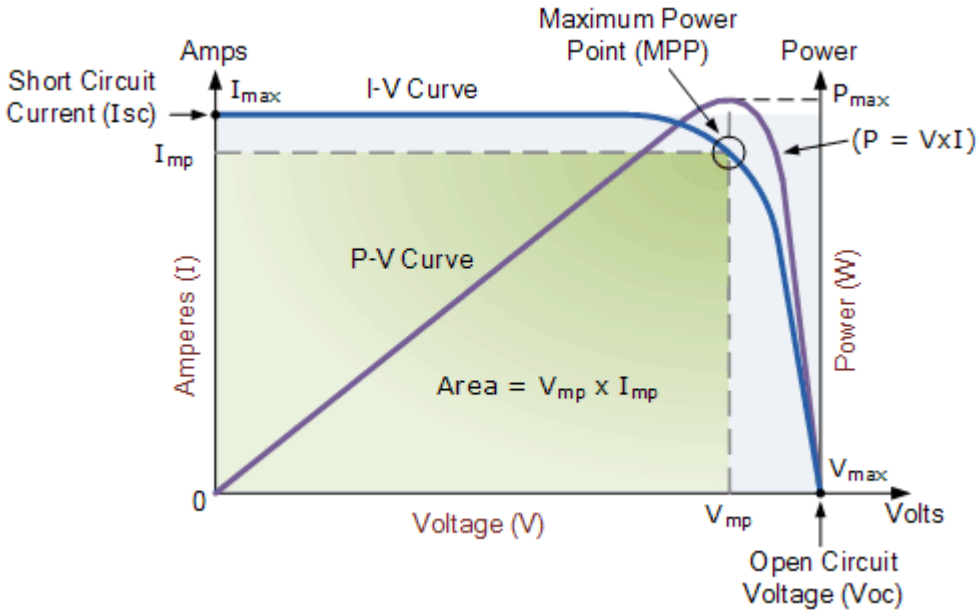

Figure 6: *Solar Cell I-V characteristic curve (Alternative Energy, 2017)*

2.3.4 Power Conversion Efficiency

The power conversion efficiency (PCE) of a solar cell is the ratio of the output energy (Pout) of the solar cell to the input energy (Pin) of the solar cell (Christiana H & Stuart B, 2017). Consequently, solar cells operate at maximum power and can achieve maximum efficiency. Pout can be taken to be $P_{MAX.}$ Solar radiant energy (P_{in}) is the product of the illuminance of the incident light, measured in W / m2 or sunlight (1000 W / m2), and has the surface of the sun. The maximum efficiency (η_{MAX}) of a solar cell can also be affected by temperature,

intensity and the spectrum of the incident light (National Instruments, 2017). The efficiency of a solar cell can be computed from the equation;

$$\eta = \frac{P_{\max}}{P_{in}} = \frac{V_{oc} I_{sc} FF}{P_{in}} \quad \text{……Equation 3}$$

2.4 Evolution of Solar Cells

2.4.1 First Generation Solar Cells

Silicon wafers are the first generation of solar cells, the advantage of silicon is that its abundant in the earth and non-toxic as well as its mature fabrication technology. 1.11 eV is the band gap of silicon and is close to the 1.3eV optimal bandgap, determined by Shockley and Queisser, with a maximum light conversion efficiency of 33% for single-junction solar cells (Wadia et al., 2009). Silicon solar cell can be monocrystalline or multi-crystalline, the silicon wafer has only one grain in a single or monocrystal solar cell while multicrystal solar cells have wafers with many grains which have distinct grain boundaries. As certified by the National Renewable Energy Laboratory (NREL) (Mitch Jacoby, 2016) the highest performance for a single crystal is 25%, and each wafer can supply 2-3 watt power (Mohammad Tawheed Kibria et al., 2015). Conventional silicon cells require ultra-high purity silicon of about 99.999%, which is monocrystalline silicon and is manufacture using crystal growth and vapour deposition techniques that consume large amounts of energy, resulting in high costs (A.Badawy, 2015). Expensive and complex technical measures have replaced single crystal wafers with polycrystalline silicon, but at the expense of solar energy conversion efficiency. Multi-crystalline silicon (mc-silicon) has a wider range of uses than monocrystalline silicon and has the potential for cost savings, so the conversion efficiency of commercially available silicon is 15-17% although a higher efficiency of 20.4% was certified by NREL in 2004 (F. Chen, 2015). The improvement of the efficiency increased the commercial viability of multi-crystalline silicon; currently, silicon has about 90% of the solar market. Continuous research in the bid to reduce cost without compromising efficiency led to the development of second-generation solar cells.

2.4.2 Second Generation Solar Cell

Second-generation solar cells can also be referred to as thin-film technology where different materials are used (A.Badawy, 2015). The material used acts as light absorbers and is

composed of thin layers. The film thickness ranges from a few nanometers (nm) to a few tens of micrometres (μm).These include copper indium gallium arsenide (CIGS), amorphous silicon (a-Si), indium cadmium selenium (CIS), cadmium telluride (CdTe), gallium arsenide (GaAs) and thin silicon films on indium tin oxide. Their energy bandgaps vary within the range of 1.1-1.7 eV (Vatansever et al., 2012). The cost is drastically reduced in the manufacturing process due to lower material consumption and low-temperature processing compared to conventional silicon since the layer of the solar cells is thin. The highest laboratory efficiency in thin film technology is 21.7% for CIGS solar cells and 21.0% for CdTe solar cells. Commercial performance over the past 10 years has increased from 9% to 16% (ISE, 2017). Flexible substrate such as glass, metals or polymers is used for thin films solar cells production which is used for Building Integrated Photovoltaics (BIPV) such as windows of houses and cars (Meilla et al., 2015). The major concerns of this technology are; high cost, lower efficiency rates, and less experience of the modules' lifetime performance (EPIA & GreenPeace, 2006) due to the scarcity and expensive nature of the elements used. The market share of all thin-film solar cells represented around 6% of the total annual production in 2016 (ISE, 2017).

2.4.3 Third Generation Solar Cell

A lot of researches are still in the process to obtain high-performance photovoltaic with a lower cost per watt of electricity generated; the cost of the inorganic materials and the fabrication technology is too high for quick commercial scale-up. These-third generation solar cells work based on Donor-Acceptor interfaces (Fru, 2016), they do not have P-N junction and are solution-processable solar cells. These include dye-sensitized solar cells, concentrated solar cells, organic solar cells, nanocrystal-based solar cells, polymer-based solar cells and tandem/multi-junction cells (Yan & Saunders, 2014). These novel technologies have the potential to contribute to sustainable energy systems but are not commercially proven yet. The production cost and raw materials of these solar cells are low but their efficiencies are low.

2.4.3.1 Organic Solar Cells

This type of photovoltaic cell technology uses organic electronics, conductive polymers or small molecules that absorb light and carry electrical charges produce electricity (Bagher,

2014). The semiconducting polymers used have suitable bandgaps, absorption characteristics, and physical properties, they are carbon-based materials comprising of alternating C-C and C=C bonds as their backbones (F. Chen, 2015). The photovoltaic effect of organic solar cells is based on the transfer of electrons from conjugated polymers of the donor type to the acceptor-type or acceptor molecules. The light-absorbing layer which comprises of the electron donor (D) and electron acceptor (A) is sandwiched between a transparent anode with a high work function for example “Indium tin Oxide (ITO) and metal cathode with a low work function” which can be magnesium or aluminum (Fru, 2016). The absorption of a photon by the donor type semiconducting polymer leads to the generation of Frankel excitons which diffuses to the donor-acceptor interface. At the interface, the strength of the effective electric field breaks up the excitons into free electrons and free holes by causing the electrons to fall from the most vacant dimensional orbit (LUMO) of the absorber material to that of the acceptor material with higher electron affinity. The holes are transported to the anode and the electrons to the cathode, generating electricity (Bastiani, 2016). Semiconducting polymers have a lower dielectric constant hence the diffusion length of excitons is shorter than that of inorganic PV materials but they have a higher extinction constant than inorganic PV. A thickness of 300nm is required by an organic material that absorbs the most incident light but has a minimum thickness of 100nm necessary to maximize light absorption (Vatansever et al., 2012). Oxidizers with high electron mobility are the best materials for polymer solar cells. Electroreceptor polymers suitable for organic solar cells include; “6,6-phenyl-C61-butric acid methyl ester ($PC_{60}BM$), 6,6-phenyl-C71-butyric acid methyl ester ($PC_{70}BM$) and poly(9,9’-dioctylfluorene-co-bis-N,N’-(4-butyl phenyl)-bis-N,N’-phenyl-1,4-phenylenediamine, (F8TB)” (Singh et al., 2005). Suitable electron donor polymers for organophosphorus compounds include poly (3-hexylthiophene) (P3HT), poly (3-octylthiophene) (P3OT), “polyphenylenevinylene (PPV), polyfluorene (PFO), poly[2,7-(9,9-dioctyl-fluorene)-alt-5,5-(4,7’-di-2-thienyl-2’,1’,3’,-benzothiadiazole) (PFODBT), poly[2-methoxy-5-(2’-ethyl-hexyloxy)-1,4-phenylene vinylene], (MEH-PPV)” (Yan & Saunders, 2014).

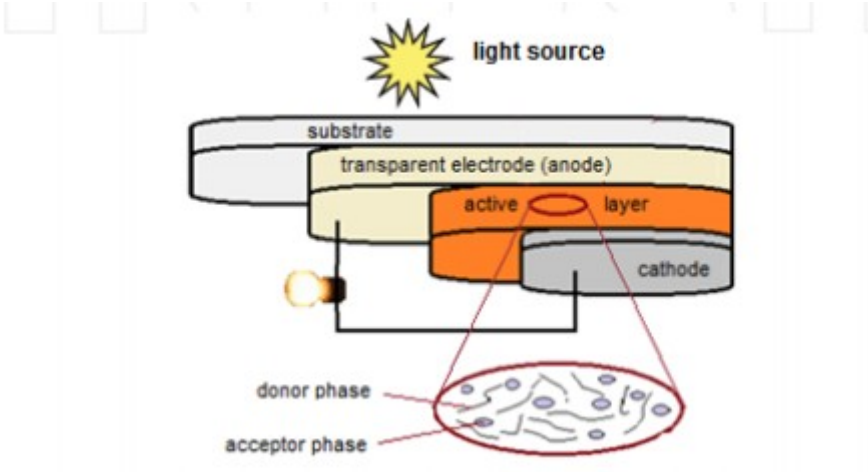

Figure7: *Donor-acceptor heterojunction configurations in a typical organic solar cell (Vatansever et al., 2012)*

2.4.3.2 Dye-sensitized solar cell

The dye-sensitized solar cell (DSSC) also known as "Gratzel cell" is considered the third-generation solar cell which was first fabricated by O'Regan and Gratzel in 1991. DSSC is a hybrid solar cell containing a mesostructured n-type inorganic oxide (eg, TiO_2) sensitized with an organic or metal complex dye and impregnated with p-type organic holes conductor (M. Liu et al., 2013). DSSCs separate the function of charge carrier transport from light absorption, the dye sensitizer absorbs the incident sunlight ray and uses the light energy to prompt electron transfer reaction (Wei, 2010). The electron is injected into the inorganic oxide (TiO_2) where it is transmitted through the TiO_2 nanoparticles to reach an electrode. DSSCs are one of the most promising classes of photovoltaic cells for the conversion of photon energy to electricity because they are inexpensive, environmentally friendly, easy to manufacture with readily available materials for their fabrication (Will Soutter, 2013). The highest efficiency record has increased from 7% in 1991 to about 14% in 2015 (C.-P. Lee et al., 2017).

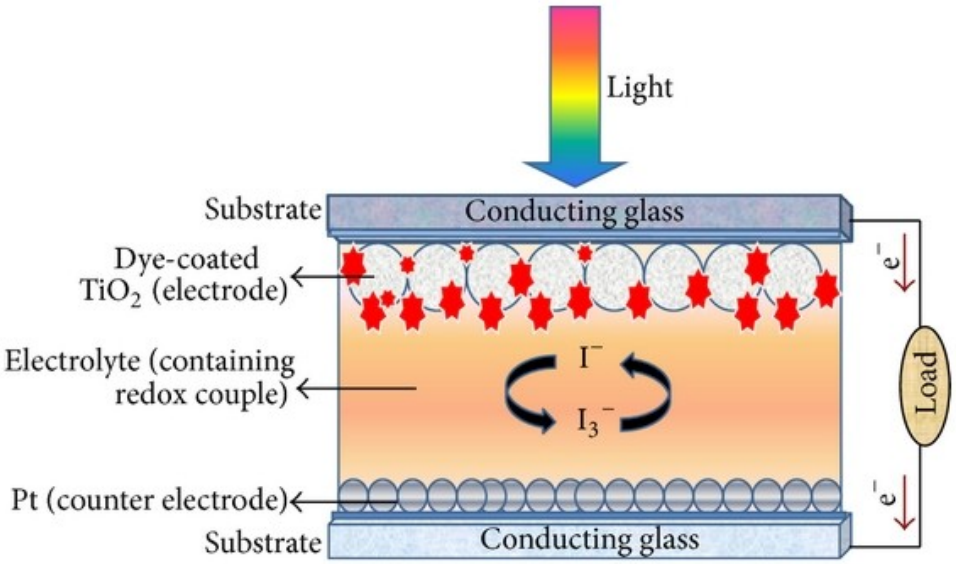

Figure 8: *Schematic illustration of a dye-sensitized solar cell (Alagarsamy Pandikumar et al., 2016)*

2.4.3.3 Quantum dot solar cell

Quantum dots (QD) are very tiny semiconductor particles or nanocrystals that are several nanometres in size (2-10 nm), their tiny nature gives their unique optical and electronic properties which differ from those of larger particles. Their optoelectronic properties are tuneable over a broad range of energy levels by changing the size of the dots, this makes it attractive for multi-junction solar cells (A.Badawy, 2015). Also, QDs have an exceptional ability to generate multiple pairs of charge carriers with a single high-energy photon (Jasim, 2015). In bulk semiconductors, the absorption of photons with energies that exceed the band gap drives electrons (hot charge carriers) from the valence band to higher levels in the conduction band. Excited electrons (hot charge carriers) are thermalized, which is a multiphoton emission, before they reach the bottom of the conduction band. With QDs, however, hot charge carriers are subjected to impact ionization (carrier multiplication) (Nozik, 2002). Hence a single absorption generates multiple electron-hole pairs called multiple exciton generation (MEG), this will lead to achieving photon-conversion efficiencies greater than 100%. This is because the absorption of UV photons by quantum dots produces more electrons than near infrared photons (Gail Overton, 2006; Jasim, 2015). Materials with a quantum dot structure can be used to create intermediate stripes. Inter-band gap solar cells are expected to achieve theoretical efficiencies of up to 65%. It allows two photons from the sub-band area to create an electron-hole pair through the intermediate region. The midway

energy band introduces additional absorption of photons, which in turn increases the photocurrent (Z. Zheng et al., 2016).

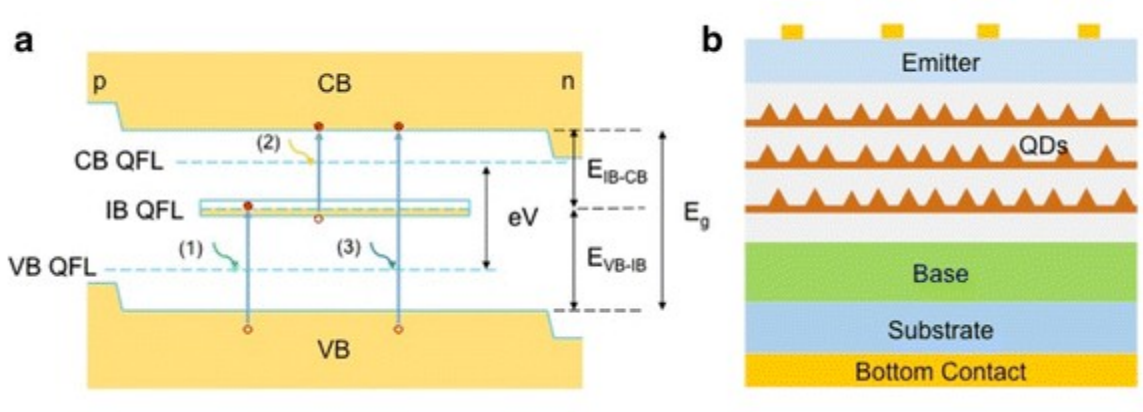

Figure 9: *Schematic illustrations of (a) an intermediate band energy level and (b) device structure of QD-Intermediate band (Z. Zheng et al., 2016)*

2.4.3.4 Tandem solar cells

Tandem solar cells (TSCs) offer higher efficiency than single junction devices by absorbing high energy photons in high bandgap cell materials, and are found under solar cells with low bandgap but high d factor. They can generate a photocurrent at higher voltages. Tandem solar cells have four main configurations, each with different degrees of optical and electrical independence (Vatansever et al., 2012). Each active ingredient used in making solar cells can convert light of a particular wavelength into electricity. To achieve better photon absorption efficiency, connect two or more active materials with a different bandgap to build a TSC. The maximum efficiency of a single cell was calculated to be 30% under non-concentrated sunlight, for tandem comprising of two sub-cells with band gaps of 1.9 and 1.0eV, the efficiency is raised to 42%. Under concentrated sunlight, the efficiencies are 40% for a single cell and 55% for tandem with two sub-cells (Ameri et al, 2009). Experimental studies on tandem solar cells, which consist of silicon cells with two III-V // transitions, have, however, achieved efficiencies of up to 32.8% with single solar lighting. An efficiency of up to 35.9% was achieved for a three-junction tandem where gallium indium phosphide/gallium arsenide (GaInP/GaAs) dual-junction cell and a Silicon single-junction were combined (Essig et al., 2017).

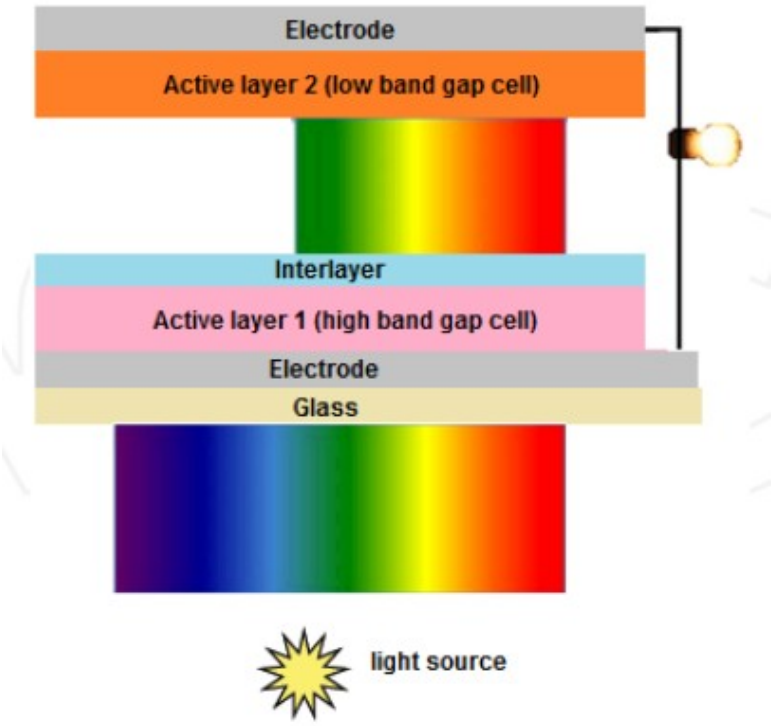

***Figure 10**: Schematic illustration of two-layer tandem junction (Vatansever et al., 2012)*

CHAPTER THREE (3)

3.0 PEROVSKITE SOLAR CELL (PSC)

Perovskite as used refers to a mineral composed of calcium titanate, with the chemical formula $CaTiO_3$. The calcium titanium oxide mineral was named after the Russian

mineralogist Lev Perovski following its discovery in the Ural Mountains of Russia by Gustav Rose in 1839 (Chen, 2015). Perovskite is also known as hybrid organic-inorganic perovskite (HOIPs) belongs to a wider class of materials with the crystal structure ABX_3. “A” and “B” are cations and “X” is an anion of different dimensions. Thus, the “A” cation is caged inside the B-X framework which is being larger than “X”. Many exciting applications are deployed for materials with this structure based on their semiconducting, “thermoelectric, insulating, piezoelectric, conducting, antiferromagnetic, and superconducting properties” (Ahmed et al., 2015). There are three major perovskite crystal structures which are; cubic, tetragonal and orthorhombic (Yifan Li, 2016).

Perovskite solar cell (PSC) is a third-generation photovoltaic technology, the prototype of perovskite structured material was noticed with the structure of a liquid DSSCs in 2009 by Miyasaka and his colleagues (Miyasaka et al, 2009). The perovskite absorber ($CH_3NH_3PbI_3$ and $CH_3NH_3PbBr_3$) replaced the conventional dye pigment in DSSCs and attained a remarkable power conversion efficiency (PCE) of 3.81 and 3.13%, respectively (Tang et al, 2017).

For methylammonium-based perovskite materials, A is an organic cation methylammonium ($CH_3NH_3^+$), Anion X is a halogen which can be; (Cl^-, Br^-,I^-) and B is a cation ($Cu^{2+,}$ Pb^{2+}, Sn^{2+}, Eu^{2+}). Currently, lead acetate ($Pb(Ac)_2$) precursor has been adapted to replace conventional lead halides(Chen et al., 2018; Zhao et al., 2016). The standard compound methylammonium lead triiodide ($CH_3NH_3PbI_3$), with mixed halides $CH_3NH_3PbI_{3-x}Cl_x$ and $CH_3NH_3PbI_{3-x}Br_x$, and use of different lead precursors such as lead acetate ($Pb(Ac)_2$) are being studied for solar cell applications (Adhikari, 2016)

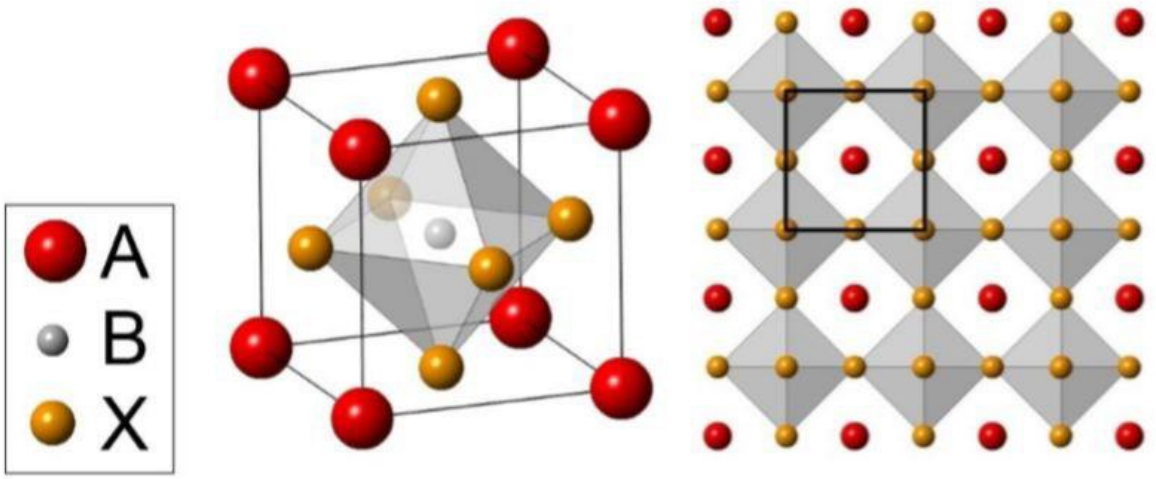

Figure 11: *The ABX_3 perovskite crystal structure (Eperon et al., 2014)*

Methylammonium lead halide perovskite ($CH_3NH_3PbI_3$) recently, has emerged as one of the most promising photovoltaic material for future photovoltaic devices owing to its outstanding optoelectronic properties as in its cost-effectiveness, ease of processability, the large light absorption coefficient, high hole mobility of $164cm^2V^{-1}S^{-1}$ and electron mobility of $24cm^2V^{-1}S^{-1}$ for $CH_3NH_3PbI_3$ single-crystal perovskite) and long charge diffusion length (~100nm) (Yifan Li, 2016). Perovskite solar cells offer unique electrical and optical properties such that, researches have been forged ahead and for only a few years, the efficiency has been improved greatly from 3.8% (Kojima et al., 2009) to 23.7% ("A Decade of Perovskite Photovoltaics," 2019), indicating that perovskite will be a very essential material in photovoltaic technology. Since the maximum theoretical PCE of the PSCs using $CH_3NH_3PbI_{3-x}Cl_x$ is 31.4%, the possibility for further improvement in the PCE stands a greater chance.

3.1 Principle of Operation of Perovskite Solar Cells and Device Structure

The Perovskite layer is used as the light-absorbing layer in the total device structure(Adhikari, 2016). The perovskite layer first absorbs photons and produces excitons (electron-hole pairs in the conduction band of titanium oxide (TiO_2), the electrons (charge carriers) are transported to the external circuit through the electron transfer layer (ETL) with the holes left been transported through the hole transfer layer (HTL) which then gather at the corresponding electrode, to form the photocurrent (Yifan Li, 2016). The literature has it that, a solid perovskite film with a thickness of hundreds of nanometers can withstand the generation of electric charges and work as ambipolar property, transporting both holes and electrons (Hsiao et al., 2015).

The conventional structures (n-i-p) and inverted structures (p-i-n) are the two basic device configurations for $CH_3NH_3PbI_3$ based solar cells. This conventional structure is normally based on Fluorine doped titanium oxide (FTO) or Indium doped titanium oxide (ITO) /compact TiO_2 (ETL)/perovskite/hole transport layer/Ag or Au (Savva et al, 2016). A highly electrical conductive conjugated polymer poly(3,4-ethylenedioxythiophene) polystyrene sulfonate (PEDOT:PSS) or (2,2′,7,7′-tetrakis(N,N-pdimethoxyphenylamino)-9,9′-spirobifluorene (spiro-OMeTAD) is used as the hole transfer layer(HTL) on the FTO/ITO substrate. Perovskite layer functions as the light-absorbing layer which is usually spin-coated on the surface of PEDOT: PSS or spiro-OMeTAD. On top of the perovskite active layer is the ETL, whose function is to transport electrons to the cathode. The last layer; cathode (silver or gold) is thermally deposited on the ETL layer (Yifan Li, 2016). The separated electrons reach to FTO electrode by moving from the conduction band of TiO_2 and holes are transported to the silver electrode by moving from the valence band of Spiro-OMeTAD or PEDOT: PSS (Adhikari, 2016). In the case of the inverted structure, the direction of flow of electrons and holes gives the differences, the current flow is reversed by changing the polarity of the electrodes, being ITO or FTO/PEDOT: PSS/Perovskite/[6,6]-Phenyl-C61-butyric acid methyl ester (PCBM)/Aluminium (Al). Usually, the ITO or FTO glass is used as the cathode while the topside layer is an anode(Savva, et al, 2016).

The conventional and inverted geometries are planar or mesoporous structures each. The mesoscopic nanostructured device has a mesoporous metal oxide layer or scaffold layer for providing mechanical support to enhance charge collection by decreasing the carrier transport distance thereby increasing absorption due to light scattering and preventing direct leakage of

current between two selective contacts (Song, et al, 2016). TiO_2 is the most commonly used n-type semiconducting oxide for mesoscopic layers in regular mesoporous geometry. TiO_2 is non-toxic, cheap, biocompatible, has a wide bandgap, and abundant. TiO_2 assists in electron transport, blocking off holes and inhibiting the recombination of the electron-hole pairs in the FTO conductive substrate in addition to the mechanical support it provides. Other mesoscopic metal oxides commonly used in addition to the TiO_2 include; Al_2O_3, ZnO and ZrO_2. Glass/FTO/cp-TiO_2/mp-TiO_2/perovskite/spiro-OMeTAD/Au and Glass/FTO/cp-TiO_2/mp-Al_2O_3/perovskite/spiro-OMeTAD/Au are examples of conventional mesoscopic architecture (Cui et al., 2016). Mesosuperstructure concept was also evaluated with ZrO_2 mesoporous scaffold (Ahmed et al., 2015). For conventional planar geometry, the perovskite is deposited directly on compact TiO_2 layer (Glass/ FTO/cp-TiO_2/perovskite/spiro-OMeTAD/ Au). Although the planar n-i-p perovskite solar cell usually exhibits enhanced V_{OC} and J_{SC} relative to a mesoscopic n-i-p device processed with the same materials and approach, the planar device usually exhibits more severe J−V hysteresis. As a result, the state-of-the-art n-i-p devices usually include a thin (~150nm) mesoporous buffer layer filled and overlaid with the perovskite (Z. Song et al., 2016).

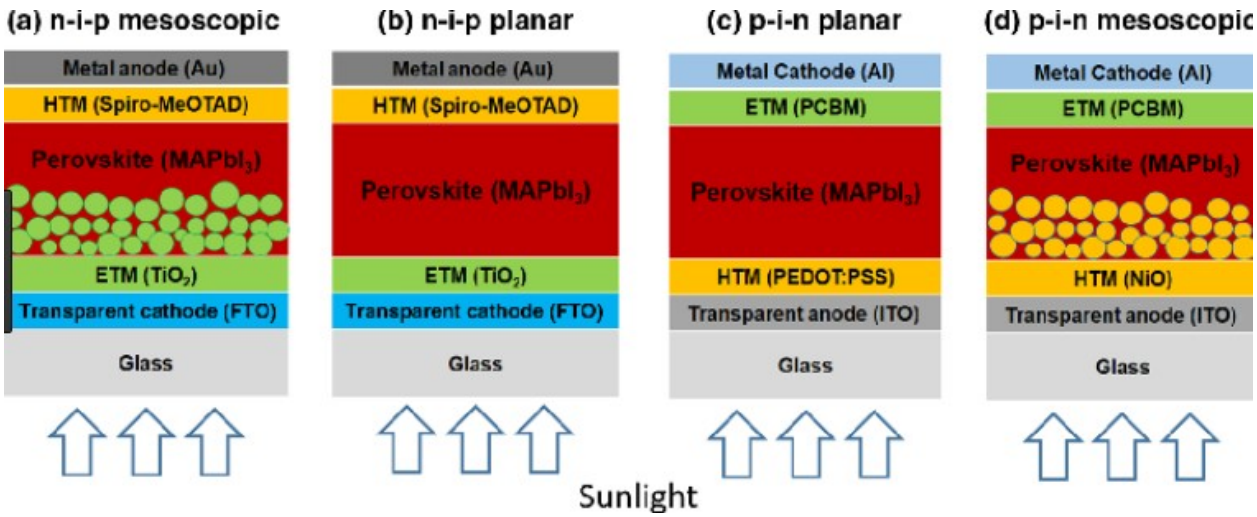

Figure 12: Schematic diagrams of perovskite solar cells in the (a) n-i-p mesoscopic, (b) n-i-p planar, (c) p-i-n planar, and (d) p-i-n mesoscopic structures. (Song, et al, 2016)

3.2 Materials

The most commonly used transparent conducting electrodes (TCO) for perovskite solar cells include indium-doped tin oxide (ITO) and fluorine-doped tin oxide (FTO). But indium is more expensive and has low mechanical resistance (Fru, 2016). Quantum Dots, Carbon

nanotubes, graphene and silver nanowires are promising materials that have been reported as transparent electrodes (Rand & Richter, 2014).

3.2.1 Hole transport materials (HTMs)

The main role of the hole-transport layer is to collect the holes and transport them out of the light absorbing perovskite layer to facilitate the separation of electron-hole pairs in the perovskite material by interaction with the electron-transport layer (D. Zhou et al., 2018). Perovskite can conduct holes but they are present at very low levels as has been reported that a hole-conductor free mesoscopic $CH_3NH_3PbI_3/TiO_2$ heterojunction PV has a PCE of 5.5%. This value is very low compared to cells with HTMs, and for efficient charge extraction, an HTM layer is of necessity (Calió et al., 2016; Fan et al., 2014). When excitons dissociate into electrons and holes, the HTM transports holes to the back electrode, which reduces recombination and increases absorption (Ahmed et al., 2015).

HTMs can be organic or inorganic material, organic HTMs includes; PEDOT: PSS, poly(3-hexylthiophene) (P_3HT), poly[bis(4-phenyl)(2,4,6-trimethylphenyl) (PTAA) and spiro-OMeTAD (Wang, et al, 2016). Spiro-OMeTAD is the most commonly used organic HTM due to its good penetration ability in the perovskite(D. Zhou et al., 2018) but is quite expensive and shows pin-holes when solution-processed. Some Scholars(J. H. Noh, N. J. Jeon, et al., 2013) adopt additives, such as 4-tert-butyl pyridine (TBP), bis (trifluoromethane), sulfonimide lithium, LTFSI to improve its holes mobility. However, the additives breakdown the perovskite layer, reducing the stability of the perovskite device; Wang et al., 2016). Inorganic HTMs include CuI, NiO, V_2O_5, $CsSnI_3$ and copper thiocyanate. They are less expensive than organic HTMs, inorganic oxide films display better environmental stability than organic HTMs but generally, organic HTLs have led to higher device efficiency. CuI shows very low efficiencies when used but copper thiocyanate is a more efficient HTM for PSCs. Qin et al. incorporated copper thiocyanate with $CH_3NH_3PbI_3$ as HTM and the device showed a PCE of 12.4% (Qin, et al, 2014). Kim et al. incorporated an inorganic HTM, NiOx giving an efficiency of 8.94% but when doped with copper to give ($Cu\text{-}NiO_x$) the efficiency increased to 15.4% (J. H. Kim et al., 2015).

3.2.2 Electron transport materials (ETMs)

ETM improves the production efficiency of photo-generated electrons and efficiently transports the electrons injected from the absorber layer (perovskite) to the electrode where

they are collected. Some inorganic metal oxides such as TiO_2, ZnO, SnO_2, SiO_2, ZrO_2, can be used as materials for ETM or scaffolding (G. Yang, et al, 2016).

The most unique property of an ETM is that it must satisfy band alignment with the perovskite layer, i.e. it should have the lowest unoccupied molecular orbital (LUMO) and highest occupied molecular orbital (HOMO) higher than the perovskite active layer. There must have high transmittance in the UV-Vis region so that a photon can pass through easily and be absorbed by the perovskite absorber (Mahmood et al., 2017). The reasons for choosing a material for electron transfer are as follows: we recommend n-type semiconductors with high charge carrier mobility. Secondly, because of the relatively large band-gap, the material must be transparent to visible light. Low-temperature preparation conditions are required to obtain the material. The most commonly used ETM for mesoporous perovskite solar cells is TiO_2, although oxygen vacancies and titanium interstitials can form in this layer. These defects cause deep sub-bandgap trap states, which reduces solar cell performance. Oxygen is required to passivate these traps; however, other layers in the device require encapsulation to prevent moisture entry which degrades the solar cell (Y. Liu et al., 2016). In addition, the rate of injection of electrons from the perovskite absorber into the ETM TiO2 is very high, but the electron mobility and transport properties are low, so the rate of electron recombination is also very high (G. Yang, et al, 2016). Pathak et al. demonstrate aluminum-doping of TiO_2 in an attempt to solve this problem, which led to an increase in device performance and stability for cells with Al-doped TiO_2 (Pathak et al., 2014). ZnO nanorods and nanoparticles were injected into the PSC as ETM with PCE 11.13% and 15.7%, respectively. However, ZnO also suffers from chemical instability (G. Yang, et al, 2016). SnO_2 is another promising ETM with wide band-gap, high transparency and high electron mobility (bulk mobility: 240 cm^2 V^{-1} s^{-1}). Li et al. used SnO_2 nanoparticle film for PSC and ETL. When combined with $TiCl_4$ treatment, the efficiency of the device exceeds 10%, but the hysteresis behavior of SnO2-based devices should be taken into account (Yi Li et al., 2015).

For organic ETMs, fullerene (C60) and its derivatives with different energy levels and electron mobilities, such as Phenyl-C61-butyric acid methyl ester (PC61BM), Indene-C60 Bisadduct (ICBA) and Phenyl-C71-butyric acid methyl ester (PC71BM), are usually used as

efficient electron extraction materials because of their low-temperature fabrication, suitable energy level alignment, and decent electron mobility.

3.2.3 Back contact materials

Metal contact materials (electrodes) are needed in perovskite solar cells to collect charge carriers and deliver them to the load where power is required, they can be inorganic semiconductor/metal or organic semiconductor/metal interface depending on the structure of the solar cell (Fru, 2016). To ensure effective collection and minimal recombination, the interface between the semiconductor and the metal must be properly engineered. Al, Ag and Au have been reported as back contact materials, Carbon has also been reported as back contact material on NiOx (M. Li et al., 2015). Other contact materials are Ni, Cr and Si (n+). Gold is the most commonly used electrode material for high-efficiency perovskite solar cells although it is expensive (Wang, et al, 2016).

3.3 Methods of Film Deposition

Thin films have a considerable influence on this age of modern energy technology. The main problem in all thin film applications depends on morphology and stability, which in turn depend on the deposition method. These deposition techniques can be physical or chemical. Among the many approaches described for synthesizing the active layer of perovskite, one-step deposition of precursor solution, two-step deposition, solvent engineering, vapour assisted solution process, sequential vapour deposition and deposition from two sources can be distinguished. A detailed description of these methods is offered below.

3.3.1 One-step spin-coating method

The easiest way to treat a perovskite growth solution is to treat the solution in one step, it involves the spin coating of a precursor solution of lead halide with a certain amount of an organic ammonium halide (Ahmed et al., 2015), uniform thin films are deposited on a flat substrate which rotates at a high speed (> 600 rpm) by the process of spin coating. The crystallites form of the perovskite grows during solvent evaporation. A post-annealing process is carried out at a relatively high temperature (around 100 °C) for the complete crystallization of the perovskite and the removal of the residual solvents. The film morphology and PSCs performance are affected by the solution concentration, precursor composition, annealing temperature, and choice of solvent (L. Zheng et al., 2015). Some

examples of solvents that are being used for the dissolution of the precursors include; dimethylformamide (DMF), gamma-butyrolactone (GBL), and dimethyl sulfoxide (DMSO). It has also been reported that the higher the concentration, the higher the coverage of the film, the more efficient the device, and the optimum concentration for solution processing as applied in the following mixture of solvents (DMF and GBL, DMF and DMSO, DMSO and GBL). This is as a result of the rapid evaporation of this combination of solvents (Ahmed et al., 2015). Im et al reported the one-step coating method for iodide perovskite active layer by reacting equimolar CH_3NH_2 and HI in the appropriate solvent. Next, the synthesized CH_3NH_3I was mixed with PbI_2 having a molar ratio of 1: 1 in GBL at 60 ° C. It was stirred for several hours and then used as a coating solution (Im, et al, 2011).

3.3.2 Two-step spin-coating method

For two-step deposition processes, the lead salt is dissolved in DMF and deposited on the substrate, when the lead iodide film is dried on a hot plate for a short time like 10 minutes, a solution of methyl ammonium iodide (MAI) dissolved in isopropyl alcohol (IPA) is used to convert the lead iodide film into perovskite (Bastiani, 2016; Liyan Yang et al., 2016). This step can be realized in very different ways: dipping the lead film into the MAI solution, spin-coating the solution MAI on top of the lead film, or exposing the lead film to MAI vapors after which the perovskite film is annealed (Bastiani, 2016).

3.3.3 Dual Source Vapour Deposition

The vapour deposition method occurs by co-evaporating the lead source and MAI in a vacuum. It makes use of vacuum technology to apply thin films of pure materials to the surface of a substrate. The crucibles containing the materials are heated to a high temperature in a vacuum (pressure < 10^{-5} Torr) either by a filament or electron-beam (e-beam) method. The material vaporizes and the vapour is transported to the target (substrate) at the top of the chamber (Sum & Mathews, 2014; L. Zheng et al., 2015). The high degree of vacuum and temperature are required which increases the cost.

3.3.4 Vapour assisted solution process

In vapour assisted solution process, the lead source is solution deposited on the substrate by spin coating, then the MAI vapour is deposited by thermal evaporation on the pre-deposited lead source (Song et al., 2015; L. Zheng et al., 2015). The advantage of the thermal evaporation method is that the perovskite film can be deposited on various substrates with

varied wettability and morphology. This precipitation method permits better control of particle morphology and size due to air-solid crystallization and effectively prevents membrane separation that can occur during liquid-solid interactions (Z. Song, et al, 2016)

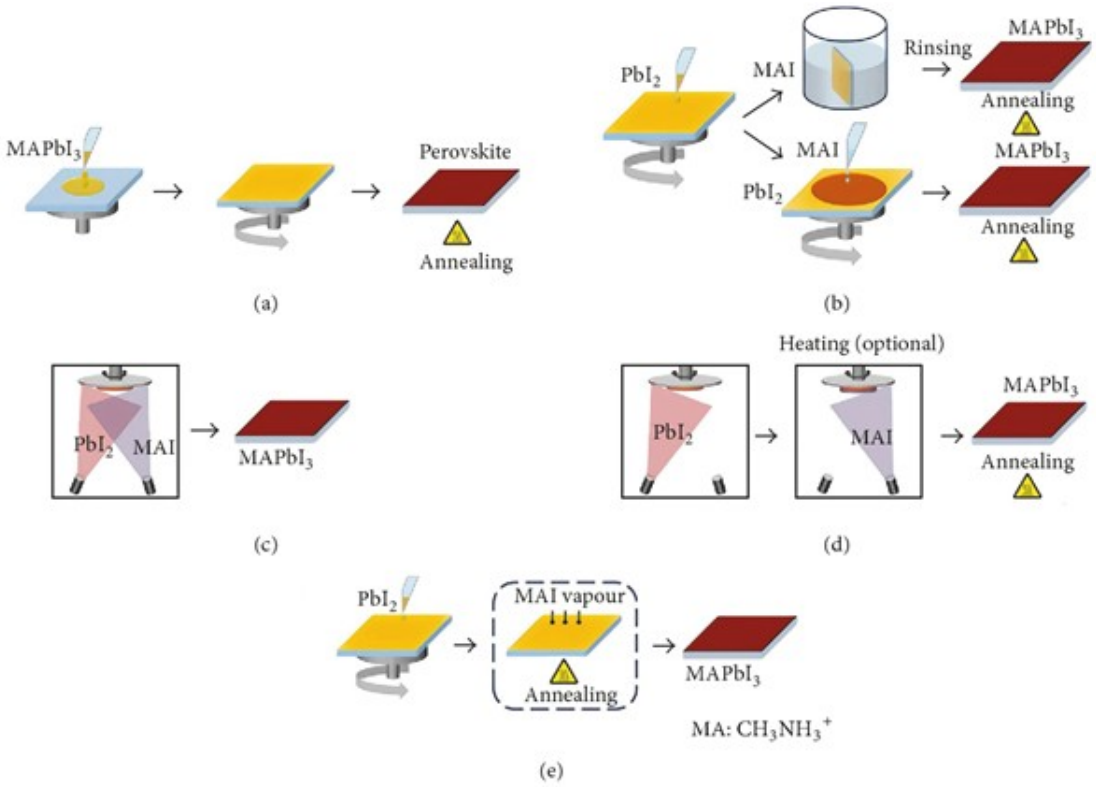

Figure 13: *Illustration of different perovskite fabrication techniques: (a) solution-based one-step technique, (b)) solution-based one-step technique, (c) dual-source vapour deposition, (d)sequential vapour-deposition method and (e) vapour-assisted solution method (Djurišić et al., 2017a)*

3.4 Stability of Perovskite

Before solar cells can be developed as commercial products, the issues of stability of perovskite devices need to be overcome. Exposure of perovskite devices to thermal-stress, ultra-violet (UV) light, oxygen, or moisture leads to the degradation of the device (Bastiani, 2016; L. Yang, et al, 2016). Upon exposure to moisture, owing to its ionic nature: water can convert the perovskite structure back to the precursor, this degradation is irreversible and occurs at the grain boundary. This is a problem for the lifetime of photovoltaic cells; as PbI_2 which is a by-product of the degradation is soluble in water and is toxic (Adhikari, 2016; Wang et al., 2016). Many approaches have been reported to increase resistance to moisture-related degradation which includes using a thin blocking layer (e.g. Al_2O_3) between the

perovskite and HTM (Dong et al., 2015), use of moisture blocking HTM (J. Liu et al., 2014), and use of hydrophobic carbon electrode(Asghar et al., 2017). A humidity of 55% will reduce the efficiency of the device, as evidenced by a colour change from dark brown to yellow (Ahmed et al., 2015). Niu and co-workers have proposed a number of chemical reactions responsible for the decomposition of $CH_3NH_3PbI_3$ in the presence of water (Guangda Niu et al., 2015)

$$CH_3NH_3PbI_{3(s)} \xleftrightarrow{H_2O} CH_3NH_3I_{(aq)} + PbI_2$$

$$CH_3NH_3I_{(aq)} \longleftrightarrow CH_3NH_{2(aq)} + HI_{(aq)}$$

$$4HI_{(aq)} + O_2 \longleftrightarrow 2I_{2(s)} + 2H_2O$$

$$2HI_{(aq)} \xleftarrow{hv} H_2\uparrow + I_{2(s)}$$

When light-soaked under AM 1.5G 1 Sun light, PSCs tend to degrade, this leads to a drop in efficiency which follows the pattern of decreasing J_{sc}. The presence of TiO_2 which is photocatalytic active for the UV light is said to be the reason for this degradation. It was proposed that UV light should be prevented from reaching the TiO_2 layer or replace the TiO_2 scaffold with another material (Asghar, et al, 2017; Wang, et al, 2016). Exposure to high temperatures also causes degradation of the perovskite layer, this is crucial as the perovskite layer requires an annealing step and the solar modules will be subjected to high temperature during temperature (Wang, et al,2016).

3.5 Morphology Perovskite Solar Cells

The morphology of the active perovskite layer strongly affects the general properties of solar cells. High coverage, uniformity and crystalline domains are favourable in achieving high power conversion efficiencies (Dualeh et al., 2014). Pinholes and grain boundaries, known as imperfect surface coatings, can result in direct contact between electrodes or charge transfer layers, which increases current loss, induces recombination, and decreased effectiveness. Generally, the morphology is influenced by the manufacturing process, perovskite composition, solvent, deposition process, and continuous post-processing (L. Yang, et al, 2016). Solution deposition of planar films of the pure hybrid perovskite materials generally results in small grain size high density of defects and low surface coverage (Zeng et al., 2017). Dual-source vacuum thermal evaporation (DSVD) and vapour-assisted solution process (VASP) are effective techniques that control crystal growth and have been used to

create smooth and uniform perovskite film (L. Yang, et al, 2016). However thermal evaporation processes are expensive due to the high temperature and vacuum needed, hence solution processes are being improved using different methods to achieve uniform films.

3.6 Methods to control the morphology of Perovskite Solar Cells

3.6.1 Solvent engineering

To control the morphology of the perovskite layer, it is important to understand and control the phase and overall formation of impurities in the mixed halide perovskite system. This is necessary for growing high quality crystals. Solvents have different evaporation rates and solubilize precursors with varying efficiencies. Various solvents and solvent additives can be used to change the uniformity and crystallinity of the perovskite membrane.

It is difficult to control the crystal structure of perovskite using a volatile solvent such as DMF (having a boiling point 153°C), higher boiling point solvents such as DMSO (189^{o}C) and GBL (204^{o}C) are usually able to create more uniform crystal domains and smoother film surfaces due to their control over the crystallinity of the inorganic PbI_2 and the subsequent reaction of PbI_2 with MAI (H.-B. Kim et al., 2014). Mixed solvents have also been used to improve film morphology, Kim et al, used a mixture of GBL and DMF (DMF: GBL 97:3 [vol %]) to create a uniform and smooth perovskite film having an efficiency of 6.16%. Jeon et al. used mixed solvents of GBL and DMSO (7:3 v/v) as processing solvent followed by toluene drop-casting a transparent CH3NH3I–PbI2–DMSO intermediate phase was formed first after the dropping of toluene using the GBL: DMSO blend solution. An extremely uniform and compact perovskite layer was formed after thermal annealing at 100^{o}C for 10 min (N. J. Jeon et al., 2014). Wang et al. investigated the effect of mixing halide using DMF and DMSO as the precursor solvents in the two-step deposition sequence, It was observed that adding DMSO to the DMF solution assisted in controlling the perovskite crystallization, resulting in enhanced PV performance (W. Li et al., 2015).

Application of solvents like toluene, dichloromethane, chlorobenzene, and chloroform during spin coating at the surface of the perovskite film leads to better concentration and uniform morphology. This is attributed to the rapid reduction of the solubility of $CH_3NH_3PbI_3$ in the mixed solvent, thus promoting fast nucleation and crystallization leading to better crystallization of perovskites, the solvent must not be able to dissolve both PbI_2 and MAI so that it cannot wash away any precursors (Z. Xiao et al., 2016). Xiao et al. developed a fast deposition crystallization (FDC) method using chlorobenzene (CB) additive to induce

crystallization during the spin coating process, the time interval between the dropping of the process solution and the solvent additive is critical to get the optimized film morphology, the best dropping time for the solvent was reported to be at the second stage (M. Xiao et al., 2014). The too early or too late dropping of CB cannot result in uniform and compact perovskite films.

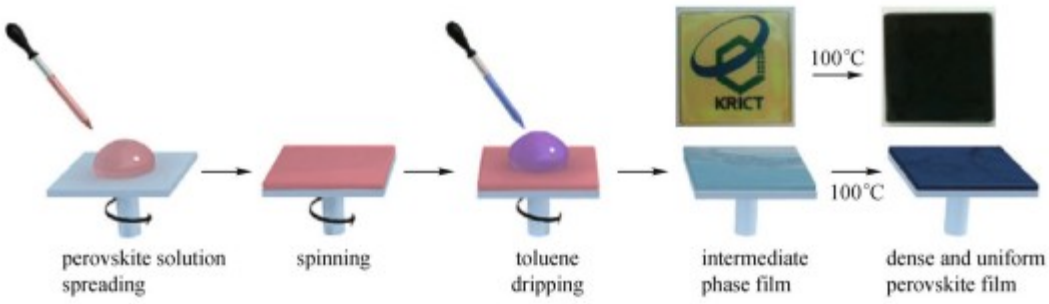

Figure 14: *Schematic representation of solvent engineering process using toluene (N. J. Jeon et al., 2014)*

3.6.2 Additives

Additives can provide fine control of the morphology of perovskite (active layer) by influencing the film formation during solution processing. They can be added to the precursor solution to enhance the PSC efficiency and long-term stability. The literature lists different types of salts for different perovskites, Peet et al. employed excess N-octylthiol for P3HT: PC_{61} (J. Peet, et al., 2006), Mei et al, used 5- ammoniumvaleric acid (5-AVA) iodide in a one-step solution for $CH_3NH_3PbI_3$ perovskite (Mei et al., 2014). The use of hydrogen iodide (HI) as an additive to perovskite of lead trihalide formamidinium has also been reported (Eperon, Stranks, et al., 2014). Leung et al. used the two-step deposition sequence for perovskite deposition, where halogen acids were added for the PbI_2 precursor solution which promoted uniform nucleation and crystal growth due to changes in PbI_2 crystal morphology (Leung et al, 2015). Jeon et al. used N-cyclohexyl-2-pyrrolidone (CHP) as an additive (5% volume ratio) in the processing solvent DMF. Highly smooth and continuous films can be obtained by using a one-step spin coating method with a 1:1 molar ratio of PbI_2 and MAI precursor solution (Y.-J. Jeon et al., 2015). Chang et al. added a small amount of polyethylene glycol which retarded the crystallization of perovskite, the film with 1wt% of polyethylene glycol gave smoother perovskite film with fewer pin-holes by using the one-step spin coating

process (Chang et al., 2015). Another distinctive additive is “4-tert-butylpyridine (TBP)”, which was added to the PbI2 precursor solution in a two-step precipitation sequence to improve the morphology of the perovskite membrane (Cohen & Etgar, 2016).

3.6.3 Thermal annealing

The thermal annealing process is another parameter for controlling the morphology of the perovskite film. The annealing of perovskite is carried out at different temperatures; it is the most applied technique that increases the crystallinity of materials, especially thin films, because of its simplicity. Qualitatively, annealing modifies the surface morphology of the perovskite film prepared by both one-step and two-step methods with temperature and time (Z. Xiao et al., 2016). Thermal annealing provides the following functions such as (1) assisting the evaporation of the excess amount of MAI and by-products (Zhang et al., 2015), (2) assisting the formation of perovskite and enhancing its crystallinity and grain growth. Excessively high annealing temperatures can grow large size perovskite grains, but tend to reduce the surface coverage, cell efficiency, and eventually decomposition of the perovskite layer (Liyan Yang et al., 2016). Eperon et al, observed that for the one-step deposited perovskite film on compact TiO_2 using 3:1 molar ratio of MAI to $PbCl_2$, as annealing temperature or duration increased, the surface coverage reduced, (Eperon, Stranks, et al., 2014). Pre-annealing, post-annealing, low-pressure vapor annealing, multi-step annealing, multiple annealing are the various reported methods of thermal annealing (Zeng et al., 2017). Moore et al. carried out a work where perovskite films were formed at 100^{o}C using the lead chloride ($PbCl_2$) and lead acetate ($PbAc_2$) as lead source and MAI as the organic precursor, and it took around 2.5 min and 43.8 min, respectively, for all the by-product to evaporate from the film since methyl ammonium acetate (MAAc) has higher volatility than methyl ammonium chloride (MACl). However, the perovskite did not form at 100^{o}C using PbI_2 as the lead source, even after 12 h of annealing, It needed much higher temperature of 150^{o}C and took 17.8 min for all the by-products (MAI) to evaporate (Moore et al, 2014). When a two-step annealing method was carried out in which annealing performed at 90 ° C for 30 minutes and then at 100 ° C for 2 minutes, it was observed that a more solid and crystalline film was formed than annealing at 100 ° C for 5 minutes (Hsu, et al, 2014).

Dualeh et al. investigated the effect of annealing temperature used in the conversion process to form perovskite material from the deposited precursor solution; they demonstrated that a

minimum temperature of 80 °C is required to form the $CH_3NH_3PbI_3$ perovskite. The highest performance was achieved for devices fabricated between 80 °C and 100 °C (Dualeh et al., 2014).

3.7. Works done on Perovskite

Miyasaka and his collaborators first reported the results of perovskite photoelectric treatment. They were drawn to the potential for self-organization of perovskite in the nanoporous TiO_2 layer of dye-sensitized solar cells (Miyasaka, et al, 2009). In 2011, Park and colleagues used similar structure in which perovskite can be deposited as hemispherically dispersed nanoparticles about 2.5 nm in diameter. By applying TiO_2 surface treatment before vapour deposition, they achieved an efficiency of 6.5% (Im, Lee, Lee, Park, & Park, 2011). Spiro-MeOTAD and mesoporous (mp) -TiO_2 are used as hole transfer materials (HTM) and electron transport chain (ETM) that also made used perovskite resulted in a PCE of 9.7% of the first perovskite-based heterojunction solar cell (H.-S. Kim et al., 2012). Lee et al., replaced mesoporous TiO_2 with mesoporous alumina (Al_2O_3) and achieved an efficiency of 10.9% (M. M. Lee, et al, 2012).

In 2013 Seok, Grätzel and colleagues also reported an efficiency of 12.0% where they used a solid perovskite capping layer overlying the scaffolding, nanoporous TiO_2 infiltrated by perovskite (Gratzel et al., 2013). Burschka used TiO_2 scaffolding and two-step iodide deposition, which improved with a confirmed efficiency of 14.1% (Burschka et al., 2013). Also, Snaith et al. fabricated planar structured perovskite solar cells with vapour-deposited perovskite layer and obtained PCE over 15% with an open-circuit voltage of 1.07V without using any mesoporous layers (M. Liu, Johnston, & Snaith, 2013). In 2014, Zhou et al. achieved an efficiency of 19.3% by fabricating perovskite solar cells under controlled humidity conditions (30 ± 5% relative humidity) with solution processing (H. Zhou et al., 2014). An efficiency of 20.2% was achieved by Yang et al., 2015 with lead formamidinium iodide ($FAPbI_3$), which has a wider absorption than conventional methyl ammonium lead iodide (W. S. Yang et al., 2015). In 2016, Saliba et al. showed a stabilized efficiency of 21.1% and 18% after 250 hours under standard operational conditions. They used a mixture of Cs/MAPbI3/FAPbI3 cation, it was shown that adding Caesium to $MAPbI_3$/$FAPbI_3$ induced uniform perovskite grains (Saliba et al., 2016).

Presently, the efficiency of perovskite solar cells is 22.1% which was achieved by Seok and colleagues through Iodide management in formamidinium-lead-halide–based perovskite layers (W. Seok. Yang et al.,2017). Wattage et al. investigated the nucleation and growth of methyl ammonium lead iodide perovskite formed by reacting pre-deposited PbI_2 thin films with different concentrations of MAI solution where they proposed that formation of perovskite films is determined by MAI concentration (Watthage, et al., 2016). Eperon et al. demonstrated that the highest photocurrents are gotten only with the highest perovskite surface coverages achieved by carefully controlling the morphology through varying process conditions (Eperon, et al., 2014).

Zhang et al. prepared Perovskite solar cells with the lead acetate $Pb(CH3COO)_2$ ($Pb(OAc)_2$) as a precursor and obtained smooth, pinhole-free perovskite films on TiO_2/FTO/glass substrates; which gave devices with power conversion of 15.2%(Zhang et al., 2015). Li et al. prepared a planar heterojunction perovskite solar cell from ($Pb(OAc)_2$) through one-step spin coating, the films derived showed enhanced surface coverage and improved photoluminescence which gave a PCE of 14.1% (Li et al., 2017). In 2016, Zhao et al. demonstrated a strategy to improve the efficiency of lead acetate based perovskite solar cell by using methyl ammonium bromide as an additive in the ($Pb(OAc)_2$) and MAI precursor solution, resulting in a uniform, compact and pin-hole free perovskite films having output efficiency of 17.6% (Zhao et al., 2016). Chen et al. prepared perovskite solar cell using ($Pb(OAc)_2$) and MAI as source materials, a suitable amount of excessive ($Pb(OAc)_2$) (about 5 mol% excessive Pb) in the solution made the film smoother with improved film crystallinity and PCE of nearly14% (Chen et al., 2018).

CHAPTER FOUR (4)

4.0 EXPERIMENTAL PROCEDURE

4.1 MATERIALS

The following materials were employed for this experiment;

- Methylammonium iodide powder (CH_3NH_3I-Sigma Aldrich, 99.99%)
- Lead (II) iodide (PbI_2), Sigma Aldrich, 99.99%
- Fluorine doped-tin oxide (FTO) coated glass
- ordinary glass
- N, N Dimethylformamide (DFM)
- Acetone
- Ethanol
- 2-isopropanol alcohol (IPA -Alfa Aesar, 99.5%)
- Distilled water

4.2 EQUIPMENT

This experimental work was carried out using the following equipment;

- Scanning electron microscope (SEM)
- Fourier Transform Infrared Radiation (FTIR)
- A High Precision, New Classic Weighing Balance (MS204S /01)
- Cost-Effective Equipment Spin Coater (Brewer Science, IS6040-PC)
- UV/VIS Spectrophotometer
- Four-point probe
- Hot plate
- Tweezers
- Magnetic stirrers

4.3 EXPERIMENTAL METHOD

The glass slides were thoroughly cleaned by dipping them in a detergent for 15 minutes in a water bath/sonicator and rinsed with distilled water. The washed glass slides were placed in acetone and left in an Ultrasonic bath for 15 minutes. The acetone containing dirt from glass slides was poured out on a hazardous waste container.

Ethanol was poured into a beaker containing the glass slides and left in an ultrasonic bath for 15 minutes. The drying gun was used in drying the glass slides.

Figure 15: Samples of glass cut using diamond tip

One-step and two-step spin coating processes were used to obtain $CH_3NH_3PbI_3$ from methylammonium iodide and lead (II) iodide

Equation showing the reaction is given below

$CH_3NH_3(s) + PbI_2(s) \rightarrow CH_3NH_3PbI_3(s)$.....1

A high precision, New Classic weighing balance (MS204S /01) was used to measure 450mg of PbI_2 and 150mg of CH_3NH_3I. This was mixed in the ratio of 1:3 in 2 ml of DFM

The solution was stirred at a temperature of 70^0C for 6 hours to ensure that a uniform solution was obtained. The Cost-Effective Equipment Spin Coater (Brewer Science, IS6040-PC) was set in three stages as follows; dispensing at 100 rpm for 10 s, thinning at 1500 rpm for the 30 s and finally dried at 500 rpm for 10s as the drying state.

Detailed Description of the Deposition Techniques is Presented Below

One Step spin coating Process

One-step solution processing is the simplest solution processing technique which involves the spin coating of a precursor solution of lead halide with a certain amount of an organic ammonium halide. For this thesis;

450 mg of PbI_2 was mixed with 150 mg of CH_3NH_3I and then dissolved in 2 ml of DMF. The solution was stirred at 350 rpm at a temperature of 70 ^{0}C over 6 hours. A transparent yellow and uniform solution was obtained. The solution was then spin-coated onto a soda-

lime glass substrate of dimensions 2.5 by 2.5 mm at the following speeds; dispensed at 100 rpm for 10 s, thinned at 1500 rpm for 30 s and dried at 500 rpm for 10s. Dispensing gives a uniform spreading of the perovskite solution, thinning determines the thickness of the sample and with the drying, all precursor residues are removed. The resulting sample was annealed at varying temperatures of 80 ^{0}C, 100 ^{0}C, and 120 ^{0}C for 20 minutes to fully form the perovskite. Also, a separate sample for the ordinary glass substrate was obtained at a spinning speed of 3000 rpm for 30 seconds and annealed at 80 ^{0}C for 20 minutes.

Two-Step spin coating Process

450 mg of PbI_2 was dissolved in 2 ml of DMF and then stirred at 350 rpm at a temperature of 70^{0}C over 6 hours to obtain a transparent yellow and uniform solution. Methyl ammonia lead iodide ($CH_3NH_3I(aq)$) solution was prepared by dissolving 150 mg of CH_3NH_3I in 2 ml of isopropyl alcohol (IPA) for 30 minutes. The PbI_2 the solution was spin-coated onto both an ordinary glass and fluorine-doped tin oxide (FTO) substrates using a two-step spin coating technique at the specified speeds as; 100 rpm for 10s at the dispensing stage, thinned at 1500 rpm for the 30 s and dried at 500 rpm for 10 s. The CH_3NH_3I solution was spin-coated onto PbI_2 at the specified speeds above. It was annealed at varying temperatures of 80 ^{0}C, 100 ^{0}C and 120 ^{0}C for 20 minutes to remove residue of IPA. Finally, the thin films formed were changed from yellow to dark brown.

Figure 16: Perovskite samples after Deposition

4.4 CHARACTERIZATION

The perovskite films formed were analyzed to study their morphology. Scanning electron microscopy (SEM-ZEISS Evo LS 10) was used to visualize the surfaces and cross-section of the perovskite films. Specord® 50 plus UV/VIS spectrometer was employed for the measurement of the optical absorption and transmittance spectrum of the perovskite thin films. The Signatone (S-302) Four-Point Probe was used to determine the current (I) and the resistance of the perovskite thin films. The sheet resistance was then determined following computations using the appropriate equations. The TI 950 Histon Triboindenter was equally used to take the surface images of the perovskite thin films and also to characterize the mechanical properties by performing indentation on the various samples.

CHAPTER FIVE (5)

5.0 RESULTS AND DISCUSSION

5.1 Ultraviolet-visible light (UV-VIS) Spectrometry

The light absorbance across the ultraviolet and visible ranges (thus, from 300 to 900 nm) of the electromagnetic spectrum is measured using the UV-VIS Spectrometer (Specord® 50 plus). The optical absorption measurement was carried out to monitor the band edge transition of the perovskite films formed. Figure 5.1A shows the absorbance of the different perovskite samples, perovskite film fabricated from PbI_2 source by the One-step spin coating method at varied temperatures did not show any remarkable absorption (i.e., figure 5.1A @ B= 80 ^{0}C, C=100 ^{0}C and D=120 ^{0}C). Perovskite fabricated by two-step spin coating technique had strong broad absorption which is evident around 500 nm in Figure 5.1B for FTO coated glass substrates. The absorption shoulder which is evident at 650nm is a result of the direct gap transition from the first valence band maximum to the conduction band minimum as observed by Xu et al., (Xu et al., 2016). The strong light-harvesting capacity could be as a

result of the quality crystals of perovskite fabricated from fluorine-doped tin-oxide coupled with the two-step technique used, the results gotten agree with previous reports (Li et al., 2017). The perovskite film formed at 80 ^{0}C and 120 ^{0}C using the same deposition technique did not have an influence on the light-harvesting capacity of the perovskite as there was no obvious improvement on the absorption curve (figure 5.2A & 5.2C).This is evident that the optimum performance of the perovskite film of both one-step and two-step occurs at 100 ^{0}C. This shows that perovskite derived from two-step spin coating technique have stronger absorbance in the entire spectra than that of perovskite films obtained from one-step spin coating technique. Also, comparing the various temperatures under each deposition technique, the red curve (@ 100 ^{0}C) peaks higher in figure 5.1A & B establishing that the optimum device performance can be observed at his temperature.

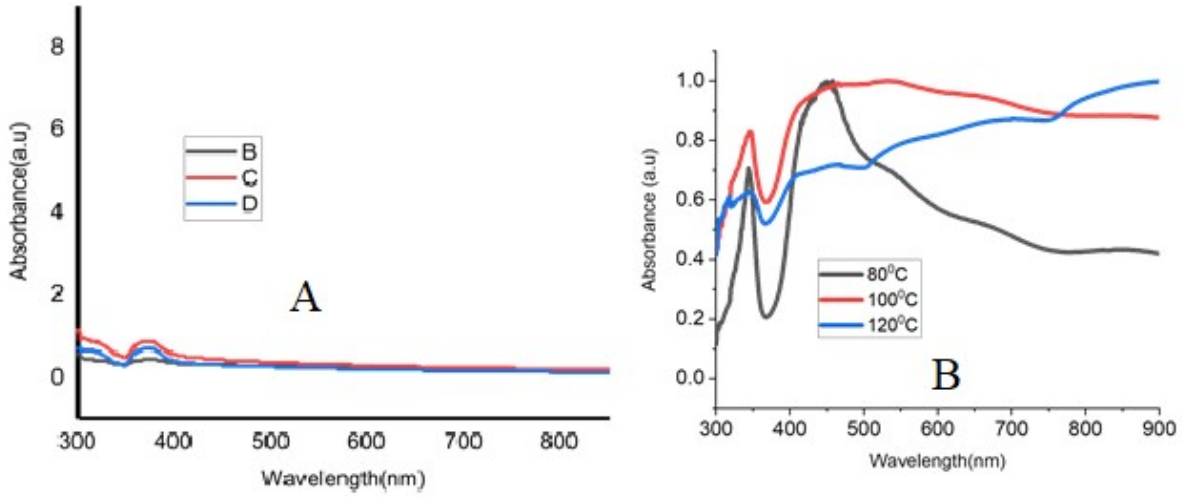

Figure 5.1: UV/VIS plot of (A) one-step and (B) two-step spin coating techniques at 80 0C, 100 0C and 120 0C

B, C and D in Figure 5.1A represent 80 ^{0}C, 100 ^{0}C and 120 ^{0}C respectively.

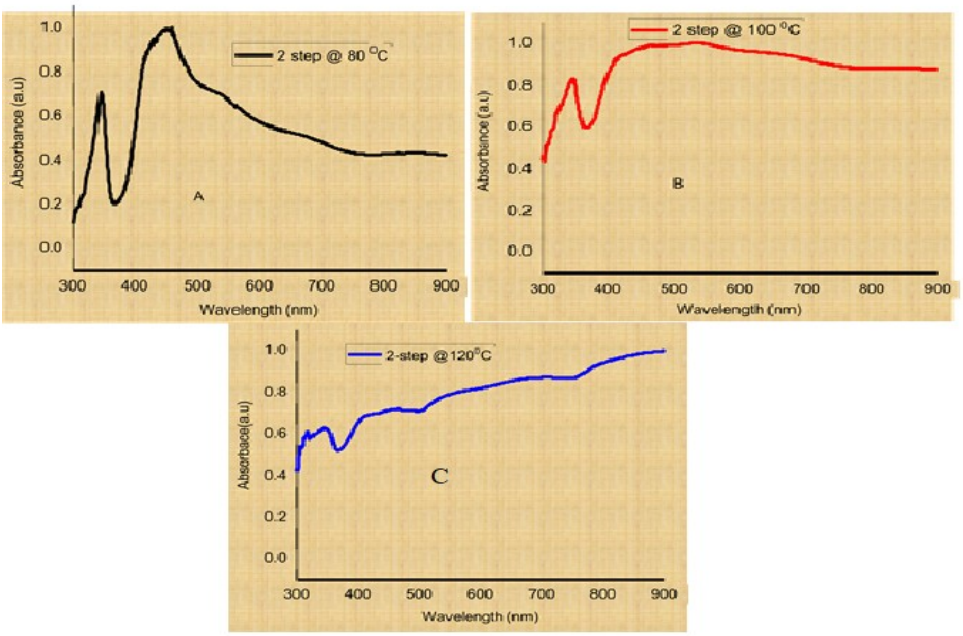

Figure 5.2:UV/VIS single plots of TSST at (A) 80 0C (B) 100 0C and (C) 120 0C.

The perovskite (Methylammonium lead iodide) is observed to have maximum absorbance at a wavelength of 500 nm in Figures 5.2A & B. A broad spectrum of absorbance can be observed around a wavelength of 900 nm indicating that the perovskite active layer is a highly efficient device and has a wide range of light-harvesting wavelength. Figure 5.2B is a single UV/VIS plot of perovskite thin-film showing the broadest device absorbance of about 550 nm wavelengths compare to that of figure 5.2A & C.

5.2 SCANNING ELECTRON MICROSCOPY

The surfaces of the fabricated perovskite films were visualized using the Scanning Electron Microscope (SEM) as shown in figure 5.3. Perovskite films were fabricated from PbI_2 source

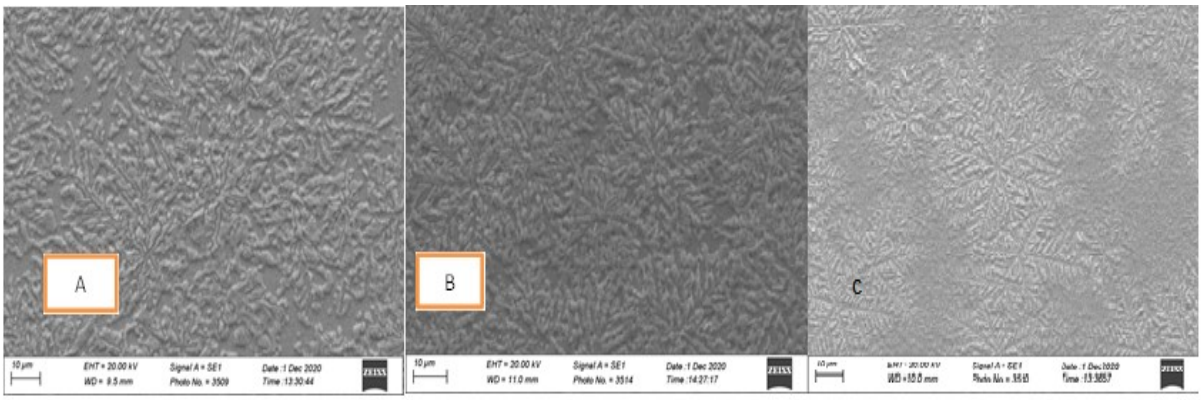

***Figure 5.3**: SEM images of $CH_3NH_3PbI_3$ on FTO coated glass substrate at; (A) 80 ^{0}C, (B) 100 ^{0}C and (C) 120 ^{0}C.*

Figure 5.3 above shows that, as the temperature increases from 80 ^{0}C to 100 ^{0}C, the surface coverage is observed to increase uniformly. But as the temperature further increased to 120 ^{0}C at C, the film uniformity on the substrate has decreased as more empty spaces are seen. This is an indication that degradation has taken place due to the fairly high temperature as reported by Kim et al. that; at high temperature $I^{+¿¿}$ and $CH_3CH_3^{+¿¿}$ diffused into the spiro-OMeTAD layer causing degradation of the electrical properties (S. Kim et al., 2017). They further established that most Perovskite Solar Cells (PSCs) employing organic HTMs degrade under thermal stress. The optimum performance of the Perovskite thin films occurs at 100 ^{0}C as determined by Chen et al. that at an optimal temperature of 100 ^{0}C, the Perovskite thin film ($CH_3NH_3PbI_2$) morphology fabricated by the two-step spin coating method has smaller grain boundaries and pin-holes than that prepared by the one-step direct annealing method which resulted in the reduction in grain boundary recombination and increase of Open-Circuit Voltage (V_{OC}) (D. Chen et al., 2017).

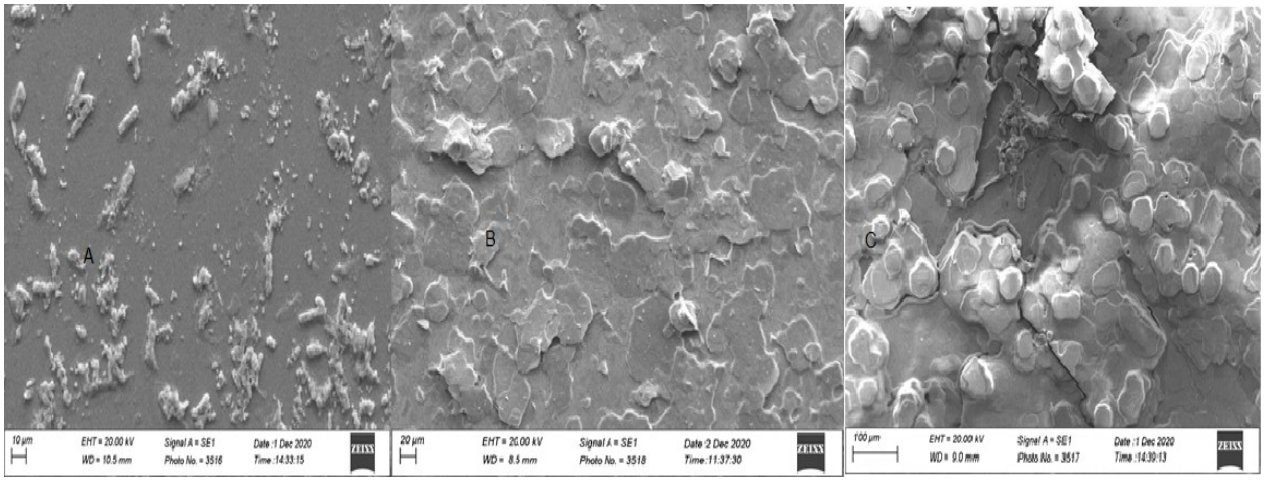

Figure 5.4: *Two-step SEM images of $CH_3NH_3PbI_3$ on FTO glass substrate at; (A) 80 ^0C (B) 100 ^0C (C) 120 ^0C.*

Perovskite thin films formed by two-step spin coating method have larger grain sizes, smoother grains and clear grain boundaries as compared to thin films produced by the one-step spin coating method. Generally looking at the SEM image of the perovskite thin films at 80 ^{0}C, one could see a more dispersed layer of perovskite thin films but at 100 ^{0}C, we can see clearer, compact, large and well- defined grains. This gives better morphology for optimum performance of perovskite devices for solar cell applications. Thus Q. Ge et al reported that the performance of perovskite-based device relies mainly on the surface morphology of the perovskite active layer (Q. Ge, J. Ding, 2016). As the temperature gets to 120 ^{0}C, more pinholes appear and the grain size becomes larger encouraging recombination at the same time reducing the quality of the film morphology.

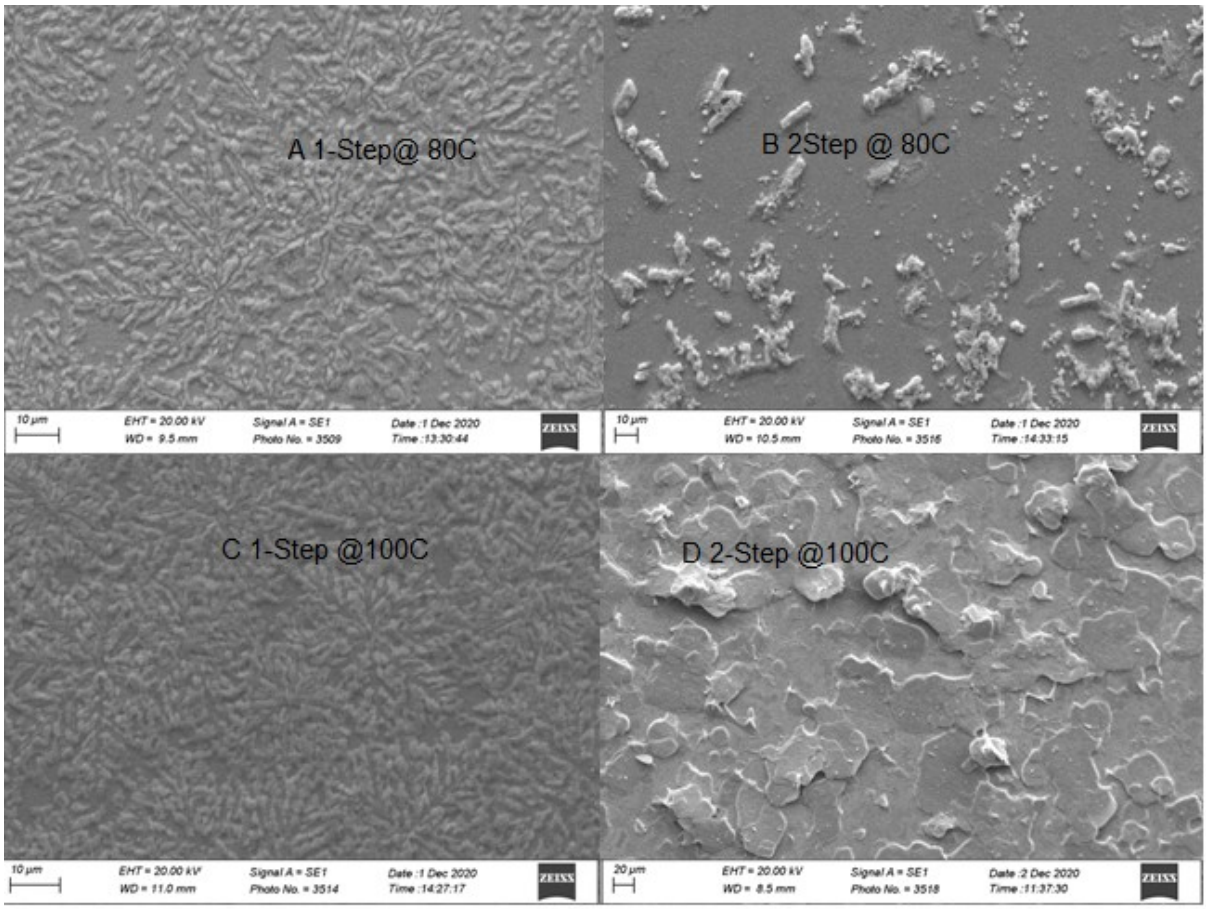
A 1-Step@ 80C
B 2Step @ 80C
C 1-Step @100C
D 2-Step @100C
10 µm EHT = 20.00 kV WD = 9.5 mm Signal A = SE1 Photo No. = 3509 Date :1 Dec 2020 Time :13:30:44
10 µm EHT = 20.00 kV WD = 10.5 mm Signal A = SE1 Photo No. = 3516 Date :1 Dec 2020 Time :14:33:15
10 µm EHT = 20.00 kV WD = 11.0 mm Signal A = SE1 Photo No. = 3514 Date :1 Dec 2020 Time :14:27:17
20 µm EHT = 20.00 kV WD = 8.5 mm Signal A = SE1 Photo No. = 3518 Date :2 Dec 2020 Time :11:37:30

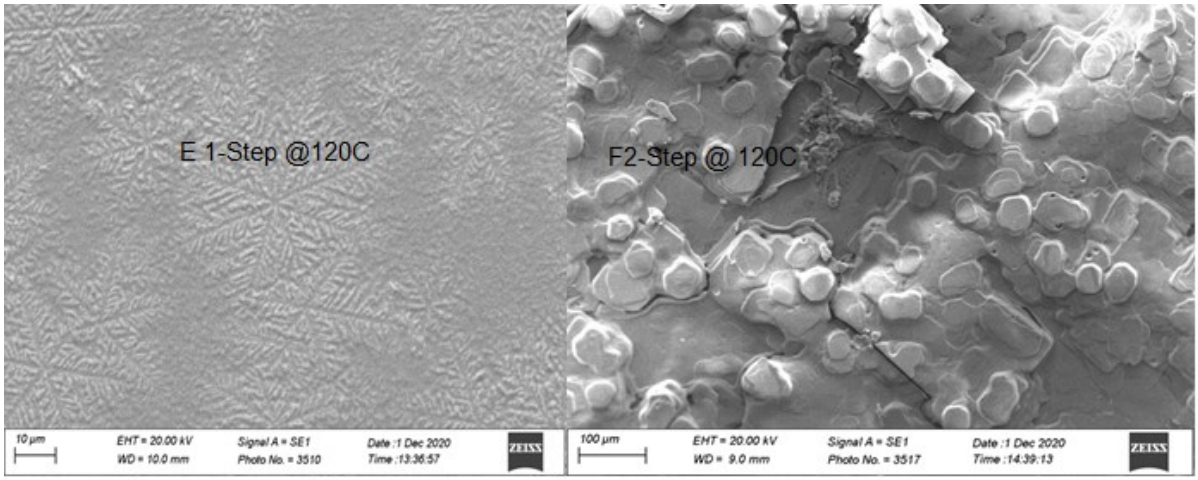
E 1-Step @120C
F2-Step @ 120C
10 µm EHT = 20.00 kV WD = 10.0 mm Signal A = SE1 Photo No. = 3510 Date :1 Dec 2020 Time :13:36:57
100 µm EHT = 20.00 kV WD = 9.0 mm Signal A = SE1 Photo No. = 3517 Date :1 Dec 2020 Time :14:39:13

Figure 5.5: *Shows the comparison between one-step and two-step spin coating methods of Perovskite thin films on FTO coated glass substrate at the same temperatures placed side by side.*

It can be observed that the absorption spectra of both thin films cover a wide range of wavelengths from visible to near-infrared region. However, perovskite thin films prepared by the Two-step spin coating (TSSC) technique resulted in a remarkably higher absorbance than that of the One-step spin coating (OSSC) at the various temperatures as established by (D. Chen et al., 2017). This could be a result of improved morphology and pure crystallinity which is consistent with the work done by (Chaudhary et al., 2020). Perovskite thin films obtained by the OSSC method contained large grain sizes and few pinholes. The pin holes could act as traps and cause the recombination of charges. The two-step spin-coated thin films showed relatively smoother surface, clearer grain boundaries and larger grain size compared to the OSSC thin films which also, conforms with what was established by Swati Chaudhary (Chaudhary et al., 2020). The TSSC thin films also cover the surface completely indicating enhanced device performance.

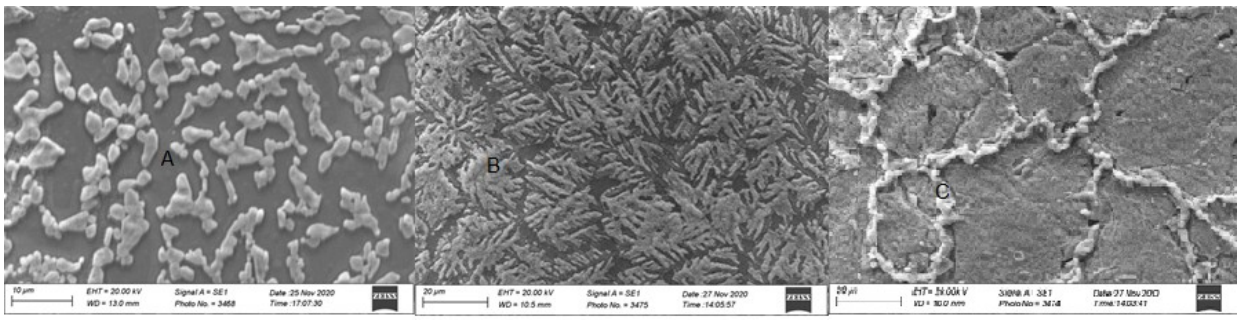

Figure 5.6: *One-step SEM images of $CH_3NH_3PbI_3$ on normal glass substrate at; (A) 80 ^{0}C, (B) 100 ^{0}C and (C) 120 ^{0}C*

We observed a dispersed surface morphology in Figure 5.6A and C than at B. There is a better surface coverage in B with little or no pinholes representing improved thin film morphology. The improved surface morphology could be a result of the fairly moderate temperature observed at B (@ 100^{0}C).

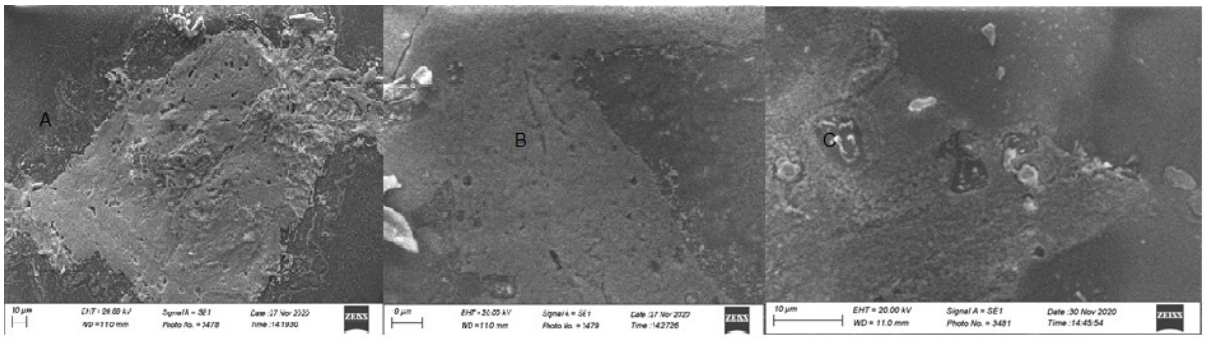

Figure 5.7: *Two-step SEM images of $CH_3NH_3PbI_3$ on normal glass substrate at; (A) 80 ^0C (B) 100 ^0C (C) 120 ^0C.*

Similarly, better surface coverage is observed in B with little or no pinholes. The improved surface morphology could be a result of the fairly moderate temperature observed at B. On the other hand, large pinholes are seen in A and C indicating that these temperatures are not ideal for optimal perovskite device performance.

Similar discussions can be made from Figure 5.5 above compared to that of figure 5.8 below, where the former is based on FTO coated glass substrate and the latter is ordinary glass. One could also observe that the adhesiveness of the perovskite thin films on the FTO coated glass substrate is far better than that on the ordinary glass substrate. Thus enhanced surface morphology and better optical absorbance are found in **figure 5.5** than in **figure 5.8**.

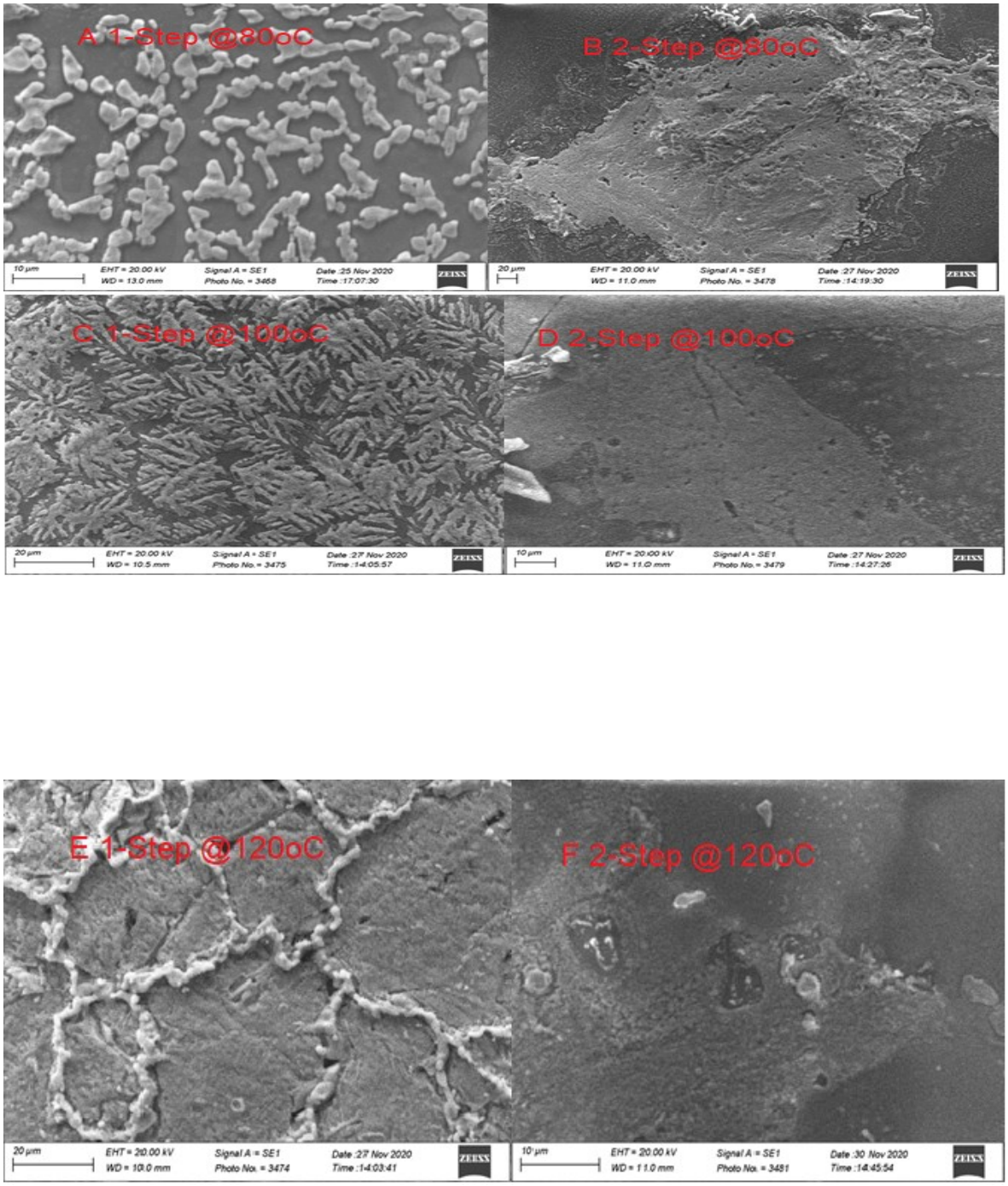

Figure 5.8: *Shows the comparison between one-step and two-step spin coating methods of Perovskite thin films on ordinary glass substrate at the same temperatures placed side by side.*

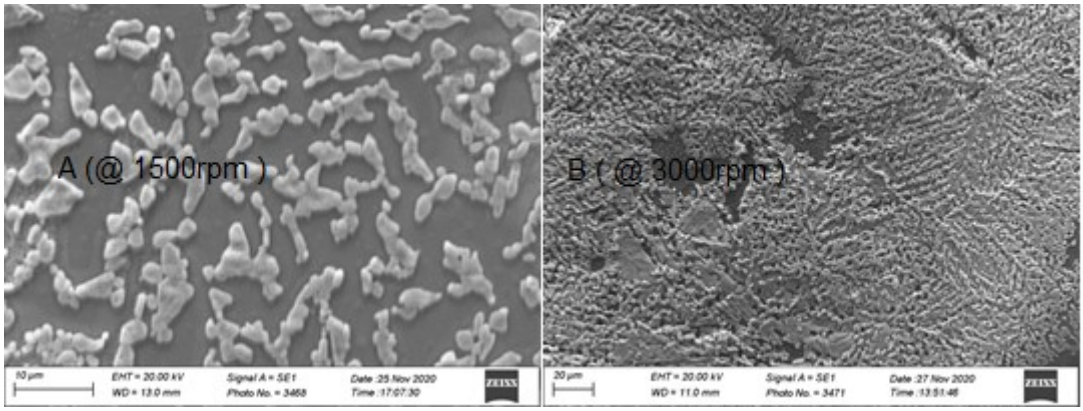

Figure 5.9: *One-step SEM images of $CH_3NH_3PbI_3$ on normal glass substrate at 80 ^0C at different spinning speeds.*

Figure 5.9 represents perovskite thin films fabricated by a one-step spin coating technique at the same temperature but with different speeds. It can be observed that the grain sizes in A are larger, clearer with well distinct grain boundaries than that at B. It implies that the slower the speed the larger the grain size and vice versa as can be seen in the image in figure 5.9A with 1500 rpm and that of B has 3000 rpm. Also, there are more pinholes in A than in B which determines the thickness of the thin films. Even though at high speed the surface coverage is better, the thin films may not give higher device performance.

5.3.0 FOUR POINT PROBE- SHEET RESISTANCE

Table 5.1: *Tabulated values of Current (I) and Resistance (Ω) for sheet resistance determination*

Temperature	Current (mA)	Resistance (Ω)
80 °C(One-step)	100	1.9940
100 °C(One-step)	100	1.7610
120 °C(One-step)	100	1.7984
80 °C (Two-step)	100	1.7980
100 °C ((Two-step)	100	1.5567
120 °C ((Two-step)	100	1.7575

5.3.1 Calculation of Sheet Resistance of the Various Perovskite Samples

Mathematically, $Rs = 4.5324 \times V/I$

Rs is ohms per square, V is voltage and I is current

We consider the Two-step spin-coated technique on FTO glass substrate

We have; I=100 mA, R=1.7980 Ω, V=?, @T=80 ^{0}C

¿ $V = IR, V = 100 \times 1.7980 = 179.80\, mV$

$$Rs = 4.5324 \times \frac{V}{I} = 4.5324 \times \frac{179.80}{100} = 8.1493\,\Omega/sq$$

@T=100^{0}C, ¿ $V = IR, V = 100 \times 1.5567 = 155.67\, mV$

$$Rs = 4.5324 \times \frac{V}{I} = 4.5324 \times \frac{155.67}{100} = 7.0556\,\Omega/sq$$

I=100mA, R=1.75750Ω, V=?,@T=120 ^{0}C

¿ $V = IR, V = 100 \times 1.7575 = 175.75\, mV$

$$Rs = 4.5324 \times \frac{V}{I} = 4.5324 \times \frac{175.75}{100} = 7.9657\,\Omega/sq$$

We now consider the One-step spin-coated technique on FTO glass substrate

I=100mA, R=1.9940Ω, V=?,@T=80^{0}C

¿ $V = IR, V = 100 \times 1.9940 = 199.40\, mV$

$$Rs = 4.5324 \times \frac{V}{I} = 4.5324 \times \frac{199.40}{100} = 9.0376\,\Omega/sq$$

I=100mA, R=1.761 0Ω, V=?,@T=100^{0}C

¿ $V = IR, V = 100 \times 1.7610 = 176.10\, mV$

$$Rs = 4.5324 \times \frac{V}{I} = 4.5324 \times \frac{176.10}{100} = 7.9816\,\Omega/sq$$

I=100mA, R=1.7984Ω, V=?,@T=120^{0}C

¿ $V = IR, V = 100 \times 1.7984 = 179.84\, mV$

$$Rs = 4.5324 \times \frac{V}{I} = 4.5324 \times \frac{179.84}{100} = 8.1511\,\Omega/sq$$

Ohms per square (Rs) are also called Wafer Sheet Resistance or Sheet Resistivity (rho) which is determined from the four-point probe.

Table 5.2: Table of computed Sheet Resistance Values for the Various Temperatures and Spin Coating Techniques

Temperature (^{0}C)	Sheet Resistance (Ω/sq)	
	Two-step	One-step
80^{0}C	8.1493	9.0376
100^{0}C	7.0556	7.9816
120^{0}C	7.9657	8.1511

Table 5.2 contained computed sheet resistivity values; it can be observed that the sheet resistance is fairly low at 100 ^{0}C for both one-step and two-step spin coating methods than the other temperatures. We observed a low sheet resistance of 7.0556Ω/sq at 100 ^{0}C for TSSC as compared to 8.1493 Ω/sq at 80 ^{0}C and 7.9657 Ω/sq at 120 ^{0}C. Low sheet resistivity implies high device performance hence the perovskite thin films fabricated showed enhanced optical and electrical properties. It can be deduced that at very low or very high temperatures, the sheet resistance of the perovskite solar cell thin films (wafers) increases, this, in turn, decreases the amount of current that would be generated by the perovskite device. Nian Chen et al., reported that the sheet resistance affects the series resistance of a solar cell and this has an impact on the field factor (FF) which in turn influences the short-circuit current density and hence the efficiency. Low sheet resistance with more gridlines yields lower series improving device efficiency (N. Chen & Ebong, 2015). The study suggests that high power conversion efficiency (PCE) of the perovskite thin films can best be observed at 100 ^{0}C which is consistent with the work obtained by Mwende Mbilol, et al. Also, samples annealed at 100 ^{0}C yielded the highest power conversion efficiency of 11.66% followed by devices annealed at 80 ^{0}C with PCE of 10.64% (Barnett et al., 2016) which conforms with what we observed in this work. When carefully viewed from the table of computed values, the sheet resistance of the perovskite thin film using TSSC at 100 ^{0}C is fairly lower (7.0556Ω/sq) than that of TSSC (7.9816Ω/sq) at the same temperature and is consistent with the fact that improved morphology leads to the decrease in; sheet resistance, band gap energy and hence,

gives excellent optical properties for high photovoltaic device performance (Mwende Mbilo1, 2019).

CHAPTER SIX (6)

6.0 CONCLUSION AND RECOMMENDATION

6.1 CONCLUSION

In conclusion, Perovskite thin films were fabricated on ordinary and FTO coated glass substrates by both one-step and two-step spin coating techniques at varying temperatures.

This was possible after uniform solutions were obtained following a thorough stirring on hotplates at 360 rpm using a magnetic stirrer. Characterization using the Scanning Electron Microscopy attached with an EDX revealed better surface morphology of perovskite thin films at 100 ^{0}C on both ordinary glass and FTO-coated glass substrate. Pinholes were observed at this same temperature on one-step perovskite thin films than that of the TSSC thin films. The better surface coverage predicts that the optimum performance of the perovskite device is achieved at 100 ^{0}C.

Similarly, the UV/VIS Spectrophotometer was used to characterize the perovskite thin films which the plot of graphs made revealed better optical absorption peaks at 100 ^{0}C than that at 80 ^{0}C and 120 ^{0}C for both OSSC and TSSC methods. Also, the UV/Vis plots showed that perovskite films deposited on fluorine-doped tin oxide substrates had stronger absorbance in the entire spectra than that of perovskite film deposited on an ordinary glass substrate.

The Four-point Probe sheet resistance measurement carried out on the various samples revealed high sheet resistivity values at 80 ^{0}C and 120 ^{0}C than at 100 ^{0}C for both OSSC and TSSC techniques. It was obtained after computing the sheet resistance from the current and voltage values measured using the four-point probe. Low sheet resistance values of 7.0556 Ω/sq and 7.9861Ω/sq for TSSC and OSSC respectively. The study suggests that the maximum performance of the perovskite thin films can best be observed at 100 ^{0}C for both OSSC and TSSC methods.

6.2 RECOMMENDATION

The future of perovskite solar cell technology appears to be brighter as efficiency continues to increase and new types of perovskite materials and compositions are developed with enhanced stability. The future of this work could be by:

- Considering the Nanomechanical Characterization of the Perovskite thin films since the TI 950 Tribo Indenter was down and we could not achieve that

- Fabricating a full perovskite solar cell device, by including HTMs, ETMs etc. using the same conditions and dimensions applied to the perovskite ($CH_3NH_3PbI_3$) active layer to enhance performance and stability.
- Considering different sources of perovskites layer in addition to the PbI_2 source.
- Considering the XRD analysis of the perovskite device to obtain maximum performance.
- Equally exploring other materials to replace lead since it toxic without compromising stability and performance.

6.3 LIMITATIONS

The following are some of the few limiting factors encountered during the Thesis write-up
The short time frame could not permit us to carry out Nanomechanical Characterization and X-ray Diffraction analysis.
Financial crisis cannot be overlooked as one of the hindrances as a result of covid-19 pandemic.

REFERENCES

A.Badawy, W. (2015). A review on solar cells from Si-single crystals to porous materials and quantum dots. *Journal of Advanced Research*, *6*(2), 123–132. https://doi.org/10.1016/J.JARE.2013.10.001

A decade of perovskite photovoltaics. (2019). *Nature Energy*, *4*(1), 20181221. https://doi.org/10.1038/s41560-018-0323-9

Adhikari, N. (2016). *Nanoscale Study of Perovskite Solar Cells for Efficient Charge Transport*.

Ahmed, M. I., Habib, A., & Javaid, S. S. (2015). Perovskite Solar Cells : Potentials, Challenges, and Opportunities. *International Journal of Photometry*, *2015*, 1–13. https://doi.org/10.1155/2015/592308

Alagarsamy Pandikumar, Su-PeiLim, SubramaniamJayabal, Nay Ming Huang, Hong Ngee Lim, & RamasamyRamaraja. (2016). Titania@gold plasmonic nanoarchitectures: An ideal photoanode for dye-sensitized solar cells. *Renewable and Sustainable Energy Reviews*, *60*, 408–420. https://doi.org/10.1016/J.RSER.2016.01.107

Alternative Energy. (2017). *Solar Cell I-V Characteristic and Solar I-V Curves*.

Ameri, T., Dennler, G., Lungenschmied, C., & Brabec, C. J. (2009). Organic tandem solar cells: A review. *Energy & Environmental Science*, *2*(4), 347. https://doi.org/10.1039/b817952b

American Chemical Society. (2014). *How a Solar Cell Works*.

Asghar, M. I., Zhang, J., Wang, H., & Lund, P. D. (2017). Device stability of perovskite solar cells – A review. *Renewable and Sustainable Energy Reviews*, *77*(July 2016), 131–146. https://doi.org/10.1016/j.rser.2017.04.003

Azpiroz, J. M., Mosconi, E., Bisquert, J. & Angelis, F. D. (2015). Defect migration in methylammonium lead iodide and its role in perovskite solar cell operation. *Energy Environ. Sci*, *8*, 2118–2127.

Bae, S. et al. (2016). Electric-Field-Induced Degradation of Methylammonium Lead Iodide Perovskite Solar Cells. *J. Phys. Chem. Lett.*, *7*, 3091–3096.

Bagher, A. M. (2014). Introduction to Organic Solar Cells. *Sustainable Energy*, *2*(3), 85–90. https://doi.org/10.12691/RSE-2-3-2

Baghzouz, Y. (2017). *Photovoltaic Devices II The p-n junction diode*.

Bai, Y. et al. (2016). Enhancing Stability and Efficiency of Perovskite Solar Cells with Crosslinkable Silane-Functionalized and Doped Fullerene. *Nature Comm, 7, 12806*.

Barnett, J. L., Cherrette, V. L., Hutcherson, C. J., & So, M. C. (2016). Effects of Solution-Based Fabrication Conditions on Morphology of Lead Halide Perovskite Thin Film Solar Cells. *Advances in Materials Science and Engineering*, *2016*. https://doi.org/10.1155/2016/4126163

Bastiani, M. De. (2016). *Ph. D. Thesis : The stability of third generation solar cells Università degli Studi di Padova*. *October*.

Burschka, J., Pellet, N., Moon, S.-J., Humphry-Baker, R., Gao, P., Nazeeruddin, M. K., & Grätzel, M. (2013). Sequential deposition as a route to high-performance perovskite-sensitized solar cells. *Nature*, *499*(7458), 316–319. https://doi.org/10.1038/nature12340

Calió, L., Kazim, S., Grätzel, M., & Ahmad, S. (2016). Hole-Transport Materials for Perovskite Solar Cells. *Angewandte Chemie International Edition*, *55*(47), 14522–14545. https://doi.org/10.1002/anie.201601757

Chang, C.-Y., Chu, C.-Y., Huang, Y.-C., Huang, C.-W., Chang, S.-Y., Chen, C.-A., Chao, C.-Y., & Su, W.-F. (2015). Tuning Perovskite Morphology by Polymer Additive for High-Efficiency Solar Cell. *ACS Applied Materials & Interfaces*, *7*(8), 4955–4961. https://doi.org/10.1021/acsami.5b00052

Chaudhary, S., Gupta, S. K., & Singh Negi, C. M. (2020). Enhanced performance of perovskite photodetectors fabricated by two-step spin coating approach. *Materials Science in Semiconductor Processing*, *109*(January), 104916. https://doi.org/10.1016/j.mssp.2020.104916

Chen, D., Zou, X., Yang, H., Zhang, N., Jin, W., Bai, X., & Yang, Y. (2017). *Effect of Annealing Process on CH 3 NH 3 PbI 3-X Cl X Film Morphology of Planar Heterojunction Perovskite Solar Cells with Optimal Compact TiO 2 Layer*. *2017*.

Chen, F. (2015). Characterization and application of Pb-based organometal halide perovskite. *Thesis Cagliari Univ.*

Chen, N., & Ebong, A. (2015). *Generalized analysis of the impact of emitter sheet resistance on silicon solar cell performance*. *August*. https://doi.org/10.7567/JJAP.54.08KD20

Chen, Q. et al. (2015). Under the spotlight: The organic-inorganic hybrid halide perovskite

for optoelectronic application. *Nano Today*, *10*, 355–396.

Chen, Y., Yerramilli, A., Shen, Y., Zhao, Z., & Alford, T. (2018). Effect of excessive Pb content in the precursor solutions on the properties of the lead acetate derived CH 3 NH 3 PbI 3 perovskite solar cells. *Solar Energy Materials and Solar Cells*, *174*, 478–484. https://doi.org/10.1016/j.solmat.2017.09.039

Christiana Honsber, & Stuart Bowden. (2017). *Solar cell fill factor*. https://doi.org/10.1016/0038-1101(81)90062-9

Christiana Honsberg, & and Stuart Bowden. (2017). *Solar Cell Efficiency | PVEducation*.

Chritiana Honsberg, & Stuart Bowden. (2017). *Short-Circuit Current | PVEducation*.

Cohen, B.-E., & Etgar, L. (2016). Parameters that control and influence the organometal halide perovskite crystallization and morphology. *Frontiers of Optoelectronics*, *9*(1), 44–52. https://doi.org/10.1007/s12200-016-0630-3

Conings, B. et al. (2015). Intrinsic Thermal Instability of Methylammonium Lead Trihalide Perovskite. *Adv. Energy Mater*, *5*, 1500477.

Cui, J., Yuan, H., Li, J., Xu, X., Shen, Y., & Lin, H. (2016). Recent progress inefficient hybrid lead halide perovskite solar cells. *And Technology of* ….

D.M. Chapin, C. S. Fuller, and G. L. P. (1954). A new silicon p-n junction photocell for converting solar radiation into electrical power. *Journal of Applied Physics*, *25*(5), 676–677.

Djurišić, A. B., Liu, F. Z., Tam, H. W., Wong, M. K., Ng, A., Surya, C., Chen, W., & He, Z. B. (2017a). Perovskite solar cells - An overview of critical issues. *Progress in Quantum Electronics*, *53*(June), 1–37. https://doi.org/10.1016/j.pquantelec.2017.05.002

Djurišić, A. B., Liu, F. Z., Tam, H. W., Wong, M. K., Ng, A., Surya, C., Chen, W., & He, Z. B. (2017b). Perovskite solar cells - An overview of critical issues. In *Progress in Quantum Electronics* (Vol. 53, pp. 1–37). Elsevier Ltd. https://doi.org/10.1016/j.pquantelec.2017.05.002

Dong, X., Fang, X., Lv, M., Lin, B., Zhang, S., Ding, J., & Yuan, N. (2015). Improvement of

the humidity stability of organic–inorganic perovskite solar cells using ultrathin Al_2O_3 layers prepared by atomic layer deposition. *Journal of Materials Chemistry A*, *3*(10), 5360–5367. https://doi.org/10.1039/C4TA06128D

Dualeh, A., Tétreault, N., Moehl, T., Gao, P., Nazeeruddin, M. K., & Grätzel, M. (2014). Effect of annealing temperature on film morphology of organic-inorganic hybrid perovskites solid-state solar cells. *Advanced Functional Materials*, *24*(21), 3250–3258. https://doi.org/10.1002/adfm.201304022

Eperon, G. E., Burlakov, V. M., Docampo, P., Goriely, A., & Snaith, H. J. (2014). Morphological control for high-performance, solution-processed planar heterojunction perovskite solar cells. *Advanced Functional Materials*, *24*(1), 151–157. https://doi.org/10.1002/adfm.201302090

Eperon, G. E., Stranks, S. D., Menelaou, C., Johnston, M. B., Herz, L. M., & Snaith, H. J. (2014). Formamidinium lead trihalide: a broadly tunable perovskite for efficient planar heterojunction solar cells. *Energy & Environmental Science*, *7*(3), 982. https://doi.org/10.1039/c3ee43822h

EPIA, & GreenPeace. (2006). *Solar Generation: Solar Electricity for over one billion people and two million jobs by 2020.* (Issue September).

Essig, S., Allebé, C., Remo, T., Geisz, J. F., Steiner, M. A., Horowitz, K., Barraud, L., Ward, J. S., Schnabel, M., Descoeudres, A., Young, D. L., Woodhouse, M., Despeisse, M., Ballif, C., & Tamboli, A. (2017). Raising the one-sun conversion efficiency of III–V/Si solar cells to 32.8% for two junctions and 35.9% for three junctions. *Nature Energy*, *2*(9), 17144. https://doi.org/10.1038/nenergy.2017.144

Etgar, L. et al. (2012). Mesoscopic CH3NH3PbI3/TiO2 Heterojunction Solar Cells. *J. Am. Chem. Soc*, *134*, 17396–17399.

Fan, J., Jia, B., & Gu, M. (2014). Perovskite-based low-cost and high-efficiency hybrid halide solar cells. *Photonics Research*, *2*(5), 111. https://doi.org/10.1364/PRJ.2.000111

Fru, J. (2016). *EFFECT OF ANNEALING TEMPERATURE ON THE FORMATION OF METHYL-AMMONIUM TIN TRI-IODIDE PEROVSKITE THIN FILM*.

Gail Overton. (2006). Quantum Dots promise - next-generation solar cells. *Photonics & Optoelectronics*, *42*(4).

Graham Zabel. (2009). *Peak People: The Interrelationship between Population Growth and Energy Resources - Resilience*.

Green Energy. (2015). *How Do Photovoltaic (PV) Solar Cells Work?*

Habisreutinger, S. N. et al. (2014). Carbon Nanotube/Polymer Composites as a Highly Stable Hole Collection Layer in Perovskite Solar Cells. *Nano Lett*, *14*, 5561–5568.

Heo, J. H., Im, S. H., Noh, J. H., Mandal, T. N., Lim, C.-S., Chang, J. A., Lee, Y. H., Kim, H., Sarkar, A., Nazeeruddin, M. K., Grätzel, M., & Seok, S. Il. (2013). Efficient inorganic-organic hybrid heterojunction solar cells containing perovskite compounds and polymeric hole conductors. *Nature Photonics*, *7*(6), 486–491. https://doi.org/10.1038/nphoton.2013.80

Hsiao, Y.-C., Wu, T., Li, M., Liu, Q., Qin, W., & Hu, B. (2015). Fundamental physics behind high-efficiency organo-metal halide perovskite solar cells. *Journal of Materials Chemistry A*, *3*(30), 15372–15385. https://doi.org/10.1039/C5TA01376C

Hsu, H.-L., Chen, C.-P., Chang, J.-Y., Yu , Y.-Y., & Shen, Y.-K. (2014). Two-step thermal annealing improves the morphology of spin-coated films for highly efficient perovskite hybrid photovoltaics. *Nanoscale*, *6*(17), 10281–10288. https://doi.org/10.1039/C4NR02751E

Hwang, I., Jeong, I., Lee, J., K, M. J. & Yong, K. (2015). Enhancing Stability of Perovskite Solar Cells to Moisture by the Facile Hydrophobic Passivation. *ACS Appl. Mater, Interfaces*, 17330–17336.

Ibn-Mohammed, T., Koh, S. C. L., Reaney, I. M., Acquaye, A., Schileo, G., Mustapha, K. B., & Greenough, R. (2017). Perovskite solar cells: An integrated hybrid lifecycle assessment and review in comparison with other photovoltaic technologies. In *Renewable and Sustainable Energy Reviews* (Vol. 80, pp. 1321–1344). Elsevier Ltd. https://doi.org/10.1016/j.rser.2017.05.095

Im, J.-H., Lee, C.-R., Lee, J.-W., Park, S.-W., & Park, N.-G. (2011). 6.5% efficient

perovskite quantum-dot-sensitized solar cell. *Nanoscale*, *3*(10), 4088. https://doi.org/10.1039/c1nr10867k

International Energy Agency. (2016). *World Energy Outlook 2016*.

ISE, F. I. for S. E. S. (2017). *Photovoltaics Report - 2017*. *July*, 44.

ITACA. (2017). *Part 2: Solar Energy Reaching The Earth's Surface | ITACA*.

J. H. Noh, N. J. Jeon, Y. C. Choi, M. K. Nazeeruddin, M. G., & and S. I. Seok. (2013). Nanostructured TiO2 /CH3NH3PbI3 heterojunction solar cells employing spiro-OMeTAD/Co-complex as hole-transporting material,". *Journal of Materials Chemistry A*, *1*(No.38), 11842–11847.

J.Peet, C.Soci, R.C.Coffin, T.Q.Nguyen, A. Mikhailovsky, D. Moses, G. Bazan. (2016). *Appl. Phys. Lett. 89*, 252105.

Jasim, K. E. (2015). Quantum Dots Solar Cells. In *Solar Cells - New Approaches and Reviews*. InTech. https://doi.org/10.5772/59159

Jeon, N. J., Noh, J. H., Kim, Y. C., Yang, W. S., Ryu, S., & Seok, S. Il. (2014). Solvent engineering for high-performance inorganic–organic hybrid perovskite solar cells. *Nature Materials*, *13*(9), 897–903. https://doi.org/10.1038/nmat4014

Jeon, Y.-J., Lee, S., Kang, R., Kim, J.-E., Yeo, J.-S., Lee, S.-H., Kim, S.-S., Yun, J.-M., & Kim, D.-Y. (2015). Planar heterojunction perovskite solar cells with superior reproducibility. *Scientific Reports*, *4*(1), 6953. https://doi.org/10.1038/srep06953

Jimoh, M. F. (2014). *Effects of Bending and Stretching on Hybrid Organic-Inorganic Trihalide Perovskite Solar Cells*. African University of Science and Technology, Abuja, Nigeria.

Keilman, N. (1998). How Accurate Are the United Nations World Population Projections? *Population and Development Review*, *24*(2019), 15. https://doi.org/10.2307/2808049

Kim, H.-B., Choi, H., Jeong, J., Kim, S., Walker, B., Song, S., & Kim, J. Y. (2014). Mixed solvents for the optimization of morphology in solution-processed, inverted-type perovskite/fullerene hybrid solar cells. *Nanoscale*, *6*(12), 6679.

https://doi.org/10.1039/c4nr00130c

Kim, H.-S., Lee, C.-R., Im, J.-H., Lee, K.-B., Moehl, T., Marchioro, A., Moon, S.-J., Humphry-Baker, R., Yum, J.-H., Moser, J. E., Grätzel, M., & Park, N.-G. (2012). Lead Iodide Perovskite Sensitized All-Solid-State Submicron Thin Film Mesoscopic Solar Cell with Efficiency Exceeding 9%. *Scientific Reports*, *2*(1), 591. https://doi.org/10.1038/srep00591

Kim, J. H., Liang, P.-W., Williams, S. T., Cho, N., Chueh, C.-C., Glaz, M. S., Ginger, D. S., & Jen, A. K.-Y. (2015). High-Performance and Environmentally Stable Planar Heterojunction Perovskite Solar Cells Based on a Solution-Processed Copper-Doped Nickel Oxide hole-transporting Layer. *Advanced Materials*, *27*(4), 695–701. https://doi.org/10.1002/adma.201404189

Kim, S., Bae, S., Lee, S. W., Cho, K., Lee, K. D., Kim, H., Park, S., Kwon, G., Ahn, S. W., Lee, H. M., Kang, Y., Lee, H. S., & Kim, D. (2017). Relationship between ion migration and interfacial degradation of CH3NH3PbI3 perovskite solar cells under thermal conditions. *Scientific Reports*, *7*(1), 1–9. https://doi.org/10.1038/s41598-017-00866-6

Kojima, A., Teshima, K., Shirai, Y., & Miyasaka, T. (2009). Organometal halide perovskites as visible-light sensitizers for photovoltaic cells. *Journal of the American Chemical Society*, *131*(17), 6050–6051. https://doi.org/10.1021/ja809598r

Lal, N. N., Dkhissi, Y., Li, W., Hou, Q., Cheng, Y. B., & Bach, U. (2017). Perovskite Tandem Solar Cells. *Advanced Energy Materials*, *7*(18), 1–18. https://doi.org/10.1002/aenm.201602761

Lee, C.-P., Li, C.-T., & Kuo-ChuanHo. (2017). Use of organic materials in dye-sensitized solar cells. *Materials Today*, *20*(5), 267–283. https://doi.org/10.1016/J.MATTOD.2017.01.012

Lee, M. M., Teuscher, J., Miyasaka, T., Murakami, T. N., & Snaith, H. J. (2012). Efficient Hybrid Solar Cells Based on Meso-Superstructured Organometal Halide Perovskites. *Science*, *338*(6107), 643–647. https://doi.org/10.1126/science.1228604

Leijtens, T. et al. (2013). Overcoming ultraviolet light instability of sensitized TiO2 with meso-super structured organometal tri-halide perovskite solar cells. *Nat. Commun*, *4*,

2885.

Li, M.H, et al. (2015). Novel spiro-based hole-transporting materials for efficient perovskite solar cells. *Chem. Commun*, *51*, *15518–*.

Li, C., Guo, Q., Wang, Z., Bai, Y., Liu, L., Wang, F., Zhou, E., Hayat, T., Alsaedi, A., & Tan, Z. (2017). Efficient Planar Structured Perovskite Solar Cells with Enhanced Open-Circuit Voltage and Suppressed Charge Recombination Based on a Slow Grown Perovskite Layer from Lead Acetate Precursor. *ACS Applied Materials & Interfaces*, acsami.7b15229. https://doi.org/10.1021/acsami.7b15229

Li, M., Shen, P., Wang, K., Guo, T., & Chen, P. (2015). Correction: Inorganic p-type contact materials for perovskite-based solar cells. *J. Mater. Chem. A*.

Li, W., Fan, J., Li, J., Mai, Y., & Wang, L. (2015). Controllable grain morphology of perovskite absorber film by molecular self-assembly toward efficient solar cells exceeding 17%. *Journal of the American Chemical Society*, *137*(32), 10399–10405. https://doi.org/10.1021/jacs.5b06444

Li, Yi, Zhu, J., Huang, Y., Liu, F., Lv, M., Chen, S., Hu, L., Tang, J., Yao, J., & Dai, S. (2015). Mesoporous SnO_2 nanoparticle films as electron-transporting material in perovskite solar cells. *RSC Advances*, *5*(36), 28424–28429. https://doi.org/10.1039/C5RA01540E

Li, Yifan. (2016). *HIGH PERFORMANCE PEROVSKITE HYBRID SOLAR CELL VIA INTERFACIAL ENGINEERING*.

Liu, J., Wu, Y., Qin, C., Yang, X., Yasuda, T., Islam, A., Zhang, K., Peng, W., Chen, W., & Han, L. (2014). A dopant-free hole-transporting material for efficient and stable perovskite solar cells. *Energy Environ. Sci.*, *7*(9), 2963–2967. https://doi.org/10.1039/C4EE01589D

Liu, M., Johnston, M. B., & Snaith, H. J. (2013). Efficient planar heterojunction perovskite solar cells by vapour deposition. *Nature*, *501*(7467), 395–398. https://doi.org/10.1038/nature12509

Liu, Y., Sun, J., Yang, Z., Yang, D., Ren, X., Xu, H., Yang, Z., & Liu, S. F. (2016). 20-mm-

Large Single-Crystalline Formamidinium-Perovskite Wafer for Mass Production of Integrated Photodetectors. *Advanced Optical Materials*, *4*(11), 1829–1837. https://doi.org/10.1002/adom.201600327

Liu, Z. (2015). *Global energy interconnection*.

M. A. Green, K. Emery, Y. Hishikawa, W. Warta, E. D. D. (2016). Prog. Photovoltaic. *Res. Appl*, *24*, 905.

Mahmood, K., Sarwar, S., & Mehran, M. T. (2017). Current status of electron transport layers in perovskite solar cells: materials and properties. *RSC Adv.*, *7*(28), 17044–17062. https://doi.org/10.1039/C7RA00002B

Marcin Majka, & Tomasz M. Majka. (2013). *Healthy light source*.

Mei, A., Li, X., Liu, L., Ku, Z., Liu, T., Rong, Y., Xu, M., Hu, M., Chen, J., Yang, Y., Gratzel, M., & Han, H. (2014). A hole-conductor-free, fully printable mesoscopic perovskite solar cell with high stability. *Science*, *345*(6194), 295–298. https://doi.org/10.1126/science.1254763

Meillaud, F., Boccard, M., G.Bugnon, Despeisse, M., & Al., S. H. et. (2015). Recent advances and remaining challenges in thin-film silicon photovoltaic technology. *Materials Today*, *18*(7), 378–384. https://doi.org/10.1016/J.MATTOD.2015.03.002

Mitch Jacoby. (2016). The future of low-cost solar cells. *American Chemical Society*, *94*(18), 30–35.

Mohammad Tawheed Kibria, Akil Ahammed, Mahmud Saad, & Shams-Ul-Islam Hossain. (2015). A Review: Comparative studies on different generation solar cell technology. *5th International Conference on Environmental Aspects of Bangladesh [ICEAB]*.

Moore, D. T., Sai, H., Wee Tan, K., Estroff, L. A., & Wiesner, U. (2014). Impact of the organic halide salt on final perovskite composition for photovoltaic applications. *APL Materials*, *2*(8), 081802. https://doi.org/10.1063/1.4886275

Mwende Mbilo1, A. O. J. and F. K. M. (2019). Correlation between the morphology and the optoelectronic and electrical properties of organometallic halide perovskite (CH3NH3MH3) thin films. *Materials Research Express*, *6*(Express 6 076431), 7.

National Geographic Society. (2017). *air mass* -.

National Instruments. (2017). *Part II – Photovoltaic Cell I-V Characterization Theory and LabVIEW Analysis Code - National Instruments*.

Niu, G. et al. (2014). Study on the stability of CH3NH3PbI3 films and the effect of post-modification by aluminum oxide in all-solid-state hybrid solar cells. *J. Mater. Chem, A 2*, 705–710.

Niu, Guangda, Guo, X., & Wang, L. (2015). Review of recent progress in the chemical stability of perovskite solar cells. *J. Mater. Chem. A*, *3*(17), 8970–8980. https://doi.org/10.1039/C4TA04994B

Nozik, A. J. (2002). Quantum dot solar cells. *Physica E: Low-Dimensional Systems and Nanostructures*, *14*(1–2), 115–120. https://doi.org/10.1016/S1386-9477(02)00374-0

Pathak, S. K., Abate, A., Ruckdeschel, P., Roose, B., Gödel, K. C., Vaynzof, Y., Santhala, A., Watanabe, S.-I., Hollman, D. J., Noel, N., Sepe, A., Wiesner, U., Friend, R., Snaith, H. J., & Steiner, U. (2014). Performance and Stability Enhancement of Dye-Sensitized and Perovskite Solar Cells by Al Doping of TiO $_2$. *Advanced Functional Materials*, *24*(38), 6046–6055. https://doi.org/10.1002/adfm.201401658

Q. Ge, J. Ding, J. L. J. et al. (2016). Promoting crystalline grain growth and healing pinholes by water vapor modulated post-annealing for enhancing the efficiency of planar perovskite solar cells. *Mater. Chem., A 4*, 13458–13467.

Qin, P., Tanaka, S., Ito, S., Tetreault, N., & Manabe, K. (2014). Inorganic hole conductor-based lead halide perovskite solar cells with 12.4% conversion efficiency. *Nature*.

Rand, B., & Richter, H. (2014). *Organic Solar Cells: fundamentals, devices, and upscaling*.

Ruy S. Bonilla, Reichel, C., Hermle, M., & Wilshaw, P. R. (2012). *Surface Passivation for Silicon Solar Cells*.

Saliba, M., Matsui, T., Seo, J.-Y., Domanski, K., Correa-Baena, J.-P., Nazeeruddin, M. K., Zakeeruddin, S. M., Tress, W., Abate, A., Hagfeldt, A., & Grätzel, M. (2016). Cesium-containing triple cation perovskite solar cells: improved stability, reproducibility and high efficiency. *Energy & Environmental Science*, *9*(6), 1989–1997.

https://doi.org/10.1039/c5ee03874j

Savva, A., Burgués-Ceballos, I., & Choulis, S. A. (2016). Improved Performance and Reliability of *p-i-n* Perovskite Solar Cells via Doped Metal Oxides. *Advanced Energy Materials*, *6*(18), 1600285. https://doi.org/10.1002/aenm.201600285

Singh, T. B., Marjanovi, N., Matt, G. J., Gü Nes, S., Sariciftci, N. S., Ramil, A. M., Andreev, A., Sitter, H., Schwö Diauer, R., & Bauer, S. (2005). *High-mobility n-channel organic field-effect transistors based on epitaxially grown C 60 films*. https://doi.org/10.1016/j.orgel.2005.03.006

Song, T.-B., Chen, Q., Zhou, H., Jiang, C., Wang, H.-H., (Michael) Yang, Y., Liu, Y., You, J., & Yang, Y. (2015). Perovskite solar cells: film formation and properties. *Journal of Materials Chemistry A*, *3*(17), 9032–9050. https://doi.org/10.1039/C4TA05246C

Song, Z., Watthage, S. C., Phillips, A. B., & Heben, M. J. (2016). Pathways toward high-performance perovskite solar cells: a review of recent advances in organometal halide perovskites for photovoltaic applications. *Journal of Photonics for Energy*, *6*(2), 022001. https://doi.org/10.1117/1.JPE.6.022001

Sten Odenwald's. (2017). *How much Energy does the sun produce in one hour*.

Sum, T. C., & Mathews, N. (2014). Advancements in perovskite solar cells: photophysics behind photovoltaics. *Energy Environ. Sci.*, *7*(8), 2518–2534. https://doi.org/10.1039/C4EE00673A

Tang, H., He, S., & Peng, C. (2017). A Short Progress Report on High-Efficiency Perovskite Solar Cells. *Nanoscale Research Letters*, *12*(1), 410. https://doi.org/10.1186/s11671-017-2187-5

Vatansever, D., Siores, E., & Shah, T. (2012). Alternative Resources for Renewable Energy: Piezoelectric and Photovoltaic Smart Structures. In *Global Warming-- Impacts and Future Perspective* (pp. 1–29). INTECH. https://doi.org/10.5772/50570

Wadia, C., Alivisatos, A. P., & Kammen, D. M. (2009). Materials availability expands the opportunity for large-scale photovoltaics deployment. *Environmental Science & Technology*, *43*(6), 2072–2077.

Wang, D., Wright, M., Elumalai, N. K., & Uddin, A. (2016). Stability of perovskite solar cells. *Solar Energy Materials and Solar Cells*, *147*, 255–275. https://doi.org/10.1016/j.solmat.2015.12.025

Watthage, S. C., Song, Z., Liyanage, G. K., Phillips, A. B., & Heben, M. J. (2016). Investigation of the nucleation and growth mechanisms of perovskite formation in the two-step solution process. *Conference Record of the IEEE Photovoltaic Specialists Conference*, *2016-Novem*, 831–834. https://doi.org/10.1109/PVSC.2016.7749723

Wei, D. (2010). Dye-sensitized solar cells. *International Journal of Molecular Sciences*, *11*(3), 1103–1113. https://doi.org/10.3390/ijms11031103

Will Soutter. (2013). *What is a Dye-Sensitized Solar Cell?*

World-nuclear association. (2017). *World Energy Needs and Nuclear Power | Energy Needs | Nuclear Energy meeting Energy Needs - World Nuclear Association*.

Xiao, M., Huang, F., Huang, W., Dkhissi, Y., Zhu, Y., Etheridge, J., Gray-Weale, A., Bach, U., Cheng, Y. B., & Spiccia, L. (2014). A fast deposition-crystallization procedure for highly efficient lead iodide perovskite thin-film solar cells. *Angewandte Chemie - International Edition*, *53*(37), 9898–9903. https://doi.org/10.1002/anie.201405334

Xiao, Z., Yuan, Y., Wang, Q., Shao, Y., Bai, Y., Deng, Y., Dong, Q., Hu, M., Bi, C., & Huang, J. (2016). Thin-film semiconductor perspective of organometal trihalide perovskite materials for high-efficiency solar cells. *Materials Science and Engineering R: Reports*, *101*, 1–38. https://doi.org/10.1016/j.mser.2015.12.002

Xu, M., Feng, J., Ou, X. L., Zhang, Z. Y., Zhang, Y. F., Wang, H. Y., & Sun, H. B. (2016). Surface Passivation of Perovskite Film by Small Molecule Infiltration for Improved Efficiency of Perovskite Solar Cells. *IEEE Photonics Journal*, *8*(5). https://doi.org/10.1109/JPHOT.2016.2608619

Yan, J., & Saunders, B. R. (2014). Third-generation solar cells: a review and comparison of polymer: fullerene, hybrid polymer and perovskite solar cells. *RSC Adv.*, *4*(82), 43286–43314. https://doi.org/10.1039/C4RA07064J

Yang, J., Siempelkamp, B. D., Mosconi, E., Angelis, F. D. & Kelly, T. L. (2015). Origin of

the Thermal Instability in CH3NH3PbI3 Thin Films Deposited on ZnO. *Chem. Mater*, *27*, 4229–4236.

Yang, G., Tao, H., Qin, P., Ke, W., & Fang, G. (2016). Recent progress in electron transport layers for efficient perovskite solar cells. *Journal of Materials Chemistry A*, *4*(11), 3970–3990. https://doi.org/10.1039/C5TA09011C

Yang, Lijun, Wang, J., & Leung, W. W.-F. (2015). Lead Iodide Thin Film Crystallization Control for High-Performance and Stable Solution-Processed Perovskite Solar Cells. *ACS Applied Materials & Interfaces*, *7*(27), 14614–14619. https://doi.org/10.1021/acsami.5b01049

Yang, Liyan, Barrows, A. T., Lidzey, D. G., & Wang, T. (2016). Recent progress and challenges of organometal halide perovskite solar cells. *Reports on Progress in Physics*, *79*(2), 026501. https://doi.org/10.1088/0034-4885/79/2/026501

Yang, W. S., Noh, J. H., Jeon, N. J., Kim, Y. C., Ryu, S., Seo, J., & Seok, S. I. (2015). High-performance photovoltaic perovskite layers are fabricated through intramolecular exchange. *Science*, *348*(6240), 1234–1237. https://doi.org/10.1126/science.aaa9272

Yang, Woon Seok, Park, B.-W., Jung, E. H., Jeon, N. J., Kim, Y. C., Lee, D. U., Shin, S. S., Seo, J., Kim, E. K., Noh, J. H., & Seok, S. Il. (2017). Iodide management in formamidinium-lead-halide–based perovskite layers for efficient solar cells. *Science*, *356*(6345), 1376–1379. https://doi.org/10.1126/science.aan2301

Zeng, W., Liu, X., Guo, X., Niu, Q., Yi, J., Xia, R., Min, Y., Kim, Y., & Kim, H. (2017). Morphology analysis and optimization: Crucial factor determining the performance of perovskite solar cells. *Molecules*, *22*(4), 1–23. https://doi.org/10.3390/molecules22040520

Zhang, W., Saliba, M., Moore, D. T., Pathak, S. K., Hörantner, M. T., Stergiopoulos, T., Stranks, S. D., Eperon, G. E., Alexander-Webber, J. A., Abate, A., Sadhanala, A., Yao, S., Chen, Y., Friend, R. H., Estroff, L. A., Wiesner, U., & Snaith, H. J. (2015). Ultrasmooth organic–inorganic perovskite thin-film formation and crystallization for efficient planar heterojunction solar cells. *Nature Communications*, *6*, 6142. https://doi.org/10.1038/ncomms7142

Zhao, L., Luo, D., Wu, J., Hu, Q., Zhang, W., Chen, K., Liu, T., Liu, Y., Zhang, Y., Liu, F., Russell, T. P., Snaith, H. J., Zhu, R., & Gong, Q. (2016). High-Performance Inverted Planar Heterojunction Perovskite Solar Cells Based on Lead Acetate Precursor with Efficiency Exceeding 18%. *Advanced Functional Materials*, *26*(20), 3508–3514. https://doi.org/10.1002/adfm.201601175

Zheng, L., Zhang, D., Ma, Y., Lu, Z., Chen, Z., Wang, S., Xiao, L., & Gong, Q. (2015). Morphology control of the perovskite films for efficient solar cells. *Dalton Trans.*, *44*(23), 10582–10593. https://doi.org/10.1039/C4DT03869J

Zheng, Z., Ji, H., Yu, P., & Wang, Z. (2016). Recent Progress Towards Quantum Dot Solar Cells with Enhanced Optical Absorption. *Nanoscale Research Letters*, *11*(1), 266. https://doi.org/10.1186/s11671-016-1457-y

Zhou, D., Zhou, T., Tian, Y., Zhu, X., & Tu, Y. (2018). Perovskite-Based Solar Cells: Materials, Methods, and Future Perspectives. *Journal of Nanomaterials*, *2018*. https://doi.org/10.1155/2018/8148072

Zhou, H., Chen, Q., Li, G., Luo, S., Song, T. -b., Duan, H.-S., Hong, Z., You, J., Liu, Y., & Yang, Y. (2014). Interface engineering of highly efficient perovskite solar cells. *Science*, *345*(6196), 542–546. https://doi.org/10.1126/science.1254050